Dynamic regulation of mRNA acetylation at synapses by learning and memory

Hai-Qian Zhou[1#], Jia-Wei Zhang[1#], Zhen Zhu[1#], Wei-Peng Lin[1,2], Yang-Yang Ding[1], Feng-Yan Dai[1], Hao-JY Jin[1], Dong-Sheng Chen[3*] and Dong-Min Yin[1,2,4*]

[1]Key Laboratory of Brain Functional Genomics, Ministry of Education and Shanghai, School of Life Science, East China Normal University, Shanghai, 200062, China

[2]Joint Center for Translational Medicine, Shanghai Fifth People's Hospital, Fudan University and School of Life Science, East China Normal University, Shanghai, 200240, China

[3]State Key Laboratory of Common Mechanism Research for Major Diseases, Suzhou Institute of Systems Medicine, Chinese Academy of Medical Sciences & Peking Union Medical College, Suzhou, 215123, China

[4]NYU-ECNU Institute of Brain and Cognitive Science at NYU Shanghai, Shanghai, 200062, China

[#]H-Q Z, J-W Z, and Z Z contributed equally to this work.

[*]Correspondence should be addressed to Prof. Dong-Sheng Chen,
Tel: 86-512-62873780
Fax: 86-512-62873779
Email: cds@ism.pumc.edu.cn

or
Prof. Dong-Min Yin,
Tel: 86-21-62232016
Fax: 86-21-62601953
Email: dmyin@brain.ecnu.edu.cn

Abstract

N4-acetylcytidine (ac4C) is the only RNA acetylation modification identified in eukaryotes and has recently been recognized as an epitranscriptomic mechanism regulating mRNA stability and translation efficiency. However, the function and regulation of mRNA acetylation in the brain remain largely unknown. In this study, the presence of ac4C in mRNA was demonstrated by dot blot analysis and UPLC-MS/MS. A transcriptome-wide mapping of ac4C was performed in the hippocampus of adult mice trained in the Morris water maze, a protocol for learning and memory. Notably, the protein levels of N-acetyltransferase 10 (NAT10), the ac4C writer, increased at synapses following memory formation but returned to baseline levels after forgetting. Moreover, the downregulation of NAT10-mediated N4-acetylcytidine in mRNA in the mouse hippocampus using the Cre/LoxP strategy resulted in impaired synaptic plasticity and deficits in learning and memory. These findings underscore the dynamics and functions of synaptic mRNA acetylation during learning and memory, providing novel insights into the epitranscriptomic regulation of brain function. The ac4C epitranscriptome dataset in mouse hippocampus is accessible via the website (http://ac4Catlas.com/).

Introduction

Learning and memory require both de novo protein synthesis and local protein synthesis at synapses[1-4]. While epigenetic regulations on DNA and histone proteins have been widely studied for learning and memory, epitranscriptomic modifications on mRNA for learning and memory have only become appreciated in recent years[5-7]. Especially, N6-methyladenosine (m6A), the most well-studied form of mRNA methylation has been shown to regulate synaptic function in learning and memory by recent studies[8].

N4-acetylcytidine (ac4C) is the only RNA acetylation modification identified in eukaryotes[9]. Initially identified in the bacterial $tRNA^{Met}$ anticodon[10], ac4C was recently detected in mRNA from mammalian cells and has been shown to promote mRNA stability and translational efficiency[11, 12]. N-acetyltransferase 10 (NAT 10) has RNA binding activity and is the only identified ac4C writer in mammalian cells[13]. NAT10-mediated ac4C has been reported to regulate tumorigenesis[14, 15], stem cell differentiation[16], cardiac remodeling[17], germ cell maturation[18]and pain signaling in the spinal cord[19, 20]. However, the function and regulatory mechanisms of ac4C in the brain remain poorly understood.

The brain region of hippocampus is critical for learning and memory[21]. The pyramidal neurons in the CA3 region of hippocampus establish a direct projection to CA1 pyramidal neurons through the Schaffer collateral (SC) pathway, known as the SC-CA1 synapse. The glutamatergic transmission at SC-CA1 synapses were augmented in mice after training in the Morris water maze (MWM)[22], a behavioral paradigm commonly used for learning and memory[23]. NAT10 has been shown to be expressed in the hippocampus and regulate depression-like behaviors[24]. However, the NAT10-regulated ac4C epitranscriptome in the hippocampus needs to be explored.

In this study, we performed ac4C-RNA immunoprecipitation (IP) followed by next-generation sequencing (acRIP-seq) and analyzed the ac4C epitranscriptome in mouse hippocampus. In addition, the ac4C modification mainly occurred in coding sequences (CDS) of mRNAs in mouse hippocampus. Intriguingly, NAT10 was found to be relocated from the cytoplasm to synapses during learning and memory. Downregulation of NAT10 in adult mouse hippocampus significantly impaired

plasticity of SC-CA1 synapses and learning and memory. Altogether these results demonstrate the dynamics and roles of synaptic mRNA acetylation during learning and memory. The dataset of ac4C epitranscriptome in mouse hippocampus is freely accessible at the website (http://ac4Catlas.com/).

Results

Detection of the presence of ac4C in mouse hippocampal poly(A) RNA

The presence of ac4C and m6A in total RNA was initially determined through ultra-high-performance liquid chromatography-tandem mass spectrometry (UPLC-MS/MS) analysis. The UPLC-MS/MS analysis revealed the ac4C stoichiometry levels (ac4C/C) at 0.657 ± 0.029% (n = 3 biological replicates) in the hippocampus of the mouse (Fig. 1a and 1d). When the hippocampus tissues were incubated with 1 mM NH2OH for 30 min before UPLC-MS/MS, a protocol of chemical deacetylation of ac4C[25], the ac4C stoichiometry levels were significantly reduced (Fig. 1b and 1d), indicating the validity of the assay. In contrast, the m6A stoichiometry levels (m6A/A) in HOM of mouse hippocampus were 0.093 ± 0.003% (n = 3 biological replicates) (Fig. 1c and 1d), which is consistent with the previous study[26]. It is known that RNA modifications are more prevalent in non-coding RNA species, such as rRNA and tRNA, compared to mRNA. ac4C, a modification identified in both rRNA and tRNA, can result in an overestimation of ac4C levels in mRNA if there is even minimal contamination from non-coding RNAs[27].

To determine whether mRNA contains ac4C, oligo(dT)-purified RNA was isolated from the hippocampus of wild-type mice. Poly(A) enrichment was confirmed by the reduced detection of 5S, 18S, and 28S rRNA relative to total RNA using UPLC-MS/MS analysis (Figures 1e and 1f). The levels of ac4C in the purified poly(A) RNA were then examined using UPLC-MS/MS techniques. The substantial enrichment of poly(A) RNA, indicated by a 90% reduction in rRNA contamination, provides compelling evidence that the detected ac4C in hippocampus poly(A) RNA is present in polyadenylated mRNA species and not a consequence of rRNA contamination. Further investigation was conducted to assess the levels of ac4C in poly(A) RNA from different

tissues. The stoichiometry of ac4C in the hippocampus was found to be significantly higher than in most other tissues, with ac4C modification levels in poly(A) RNA being similar to those of m6A (Figure 1i). This observation was further supported by a standard curve generated using UPLC-MS/MS, which confirmed the accuracy and sensitivity of the method in detecting ac4C modifications (Figure 1g). Chromatograms of ac4C standards and ac4C in poly(A) RNA provided additional validation (Figure 1h).

These analyses provide compelling evidence for the presence of ac4C in poly(A) RNA in the hippocampus. This suggests a potential role for this modification in regulating mRNA stability and translation efficiency within this brain region. The results provide robust evidence for the specific detection of ac4C in mRNA, significantly reducing the likelihood of interference from other RNA species.

Changes of mRNA acetylation in mouse hippocampus during learning and memory

We used the protocol of MWM[28] to explore how learning and memory regulate mRNA acetylation in mouse hippocampus. The control mice were placed in an atypical MWM with a visible platform once a day for 2 days, and thus could reach the visible platform in the target region without training (Extended Data Fig. S1a and S1b). However, the control mice failed to recall the target region during the probe test on day 6 (Extended Data Fig. S1c). Conversely, the learning mice were trained in a classical MWM with a hidden platform (Extended Data Fig. S1d and S1e). The learning mice took 5 training days to remember the target region during the probe test on day 6 (Extended Data Fig. S1f), indicative of memory formation. As expected from previous research[29], the learning mice could not remember the target region during the probe test on day 20 (Extended Data Fig. S1g), indicating that memories were forgotten (Extended Data Fig. S1h).

Given that mRNA is localized not only in the homogenates (HOM) but also at synapses of the brain[30], we isolated the synaptosome (SYN) fraction from mouse hippocampus. This fraction was enriched for synaptic proteins (PSD95 and synapsin 1) and depleted of cytoplasm-restricted (the S2 fraction) protein (α-tubulin) (Fig. 2a).

121 Further analysis using ac4C dot-blots revealed comparable ac4C mRNA levels in SYN
122 between control and learning mice on days 1, 6 and 20 (Fig. 2b-d). The results showed
123 similar ac4C levels of poly(A) RNA in SYN of the hippocampus between control and
124 learning mice on days 1 and 20. Notably, ac4C-modified poly(A) RNA significantly
125 increased in SYN of learning mice on day 6, relative to controls (Fig. 2e).

126 We mapped ac4C sites on hippocampal mRNAs at days 1, 6, and 20 using acRIP-
127 seq methods (Extended Data Fig. S7a). Three libraries (input, IgG-IP and ac-IP) were
128 sequenced for each biological replicate. The acRIP-seq reads were mapped to the mouse
129 synaptic and homogenate transcriptome[8] to identify regions of enrichment relative to
130 input and IgG-IP, and the fold enrichment (FE) of an ac4C peak was defined as ac-IP /
131 input (Extended Data Fig. S2a). The limited yield of mRNA from the SYN (100 ng per
132 mouse hippocampus, 1/100th that required) presented challenges using existing acRIP-
133 seq protocols[31]. We established a low-input acRIP-seq protocol to use submicrogram
134 input by enhancing sample quantification, optimizing immunoprecipitation, and
135 conducting a SMARTer cDNA synthesis step before library construction. Our protocol
136 reliably produced input and IP libraries for SYN using hippocampal RNA from ten mice.
137 By contrast, we produced input and IP libraries using hippocampal RNA from three
138 mice for HOM.

139 The differences in normalized mapped ratios across the three libraries (IP, Input,
140 and IgG) effectively demonstrate the stability and reliability of the conventional acRIP
141 sequencing method (Extended Data Fig.S2b). A total of 7217ac4C mRNAs identified
142 in at least two biological replicates of HOM were considered reliable while its 11061
143 peaks were also subjected to further analysis (Extended Data Fig. S2c and d). Input for
144 HOM with biological replicates were evaluated using Pearson's r2 (Extended Data Fig.
145 S2e). Biological triplicates of acRIP-seq, using purified hippocampal poly(A) RNA,
146 yielded common peaks with the TCCTCC consensus sequence and enrichment at the
147 coding sequence and 5′UTR (Extended Data Fig. S2f–g) on transcripts. Although SYN
148 did not include biological replicates, the acRIP sequencing was conducted using 10
149 mice per group. The substantial sample size, coupled with stringent quality control and
150 calibration procedures, compensated for the lack of replicates and ensured the

robustness and reliability of the results.

Through stringent quality control measures, we further calibrated our findings against three previously published synaptic gene databases, selecting the most reliable mRNAs in each group to calculate total ac4C modification per mRNA[32-34]. We defined the mRNAs with identified ac4C modifications as ac4C-mRNAs.

Subsequently, we evaluated all ac4C modifications occurring on each mRNA as ac4c-mRNA fold enrichment. The cumulative distribution and box plot analysis of ac4C-mRNA fold enrichment on days 1, 6, and 20 demonstrated changes in acetylation levels corresponding to the formation and forgetting of memory (Fig 2. f-h). On day 6, the acetylation levels of mRNA in the SYN of the hippocampus were significantly higher in mice with confirmed memory formation, as seen in the probe test, compared to the control group. To eliminate the possibility of false positives due to changes in mRNA content, we measured mRNA expression levels on days 1, 6, and 20 (Fig. 2 i-k). The results showed no significant changes in mRNA expression levels at SYN in the hippocampus at any of the three time points. In addition, ac4C dot-blots revealed identical ac4C mRNA levels in HOM between control and learning mice on days 6 (Extended Data Fig. S3a). The results showed similar ac4C levels of poly(A) RNA in SYN of the hippocampus between control and learning in the HOM. Moreover, in the Hom group, there were no significant differences in the levels of ac4C mRNA acetylation and normalized mRNA expression between the control and learning mice on day 6. Based on these results, we showed that learning and memory processes are closely linked to increased levels of ac4C at SYN rather than HOM.

Expression of Nat10 in the neurons of mouse hippocampus

Nat10 is currently the only known ac4C writer and is a key factor in the observed alterations of acetylation modifications; however, its expression patterns in the hippocampal region of the brain remain unknown. Since the commercially available NAT10 antibodies are not suitable for immunostaining in mouse hippocampus, we took use of the strategy of genetic labeling[35, 36] to investigate the expression pattern of Nat10. To this end, a heterozygous knockin mouse line ($Nat10^{Cre/+}$) that expressed the Cre

recombinase right after the start codon (ATG) of Nat10 gene was generated using the CRISPR/Cas9 techniques (see details in the method). Since the Cre recombinase and Nat10 share the same regulatory elements for gene expression in the Nat10$^{Cre/+}$ mice, the Nat10 expression pattern can be revealed through the Cre-reporting adeno-associated virus (AAV) that express EGFP in a Cre-dependent manner. (Fig. 3a).

The dorsal hippocampus integrates multiple synaptic inputs from other brain regions and is critical for learning and memory[37-39]. To study the expression pattern of Nat10 in the dorsal hippocampus of adult mice, 7-week-old Nat10$^{Cre/+}$ mice were recruited for AAV injection, and the EGFP expression was analyzed 3 weeks later (Fig. 3b). Nat10 was mainly expressed in the pyramidal cell layer (sp) of CA1 region and granule cell layer (gcl) of dentate gyrus (DG) (Fig.3c). Most of the Nat10-expressing cells are mature neurons, as shown by the overlay between EGFP and NeuN, a protein marker for mature neurons (Fig. 3d-e). Moreover, most of the Nat10-positive cells are excitatory pyramidal neurons in the CA1 region of mouse hippocampus, indicated by the co-localization of EGFP with Neurogranin (NG), a protein marker for excitatory pyramidal neurons (Fig. 3f and g). Altogether these results indicate that Nat10 is mainly expressed by mature excitatory neurons in adult mouse hippocampus.

Increased of NAT10 proteins in SYN after learning and memory

The above data showed that a dynamic increase in ac4C levels specifically at synaptosome, rather than in homogenates, in the hippocampus of mice after learning and memory training. Next, we aim to investigate whether the protein levels of NAT10 in SYN are also regulated by learning and memory. Toward this aim, we purified SYN from the hippocampus of control and learning mice at different time points after MWM training and analyzed the protein levels of NAT10 by western blots (Fig. 4a). The protein levels of NAT10 in SYN were similar between control and learning mice on day 1 (Fig. 4b). Interestingly, the protein levels of NAT10 were significantly increased in SYN of learning mice on day 6, compared with controls (Fig. 4c), but returned to normal levels on day 20 (Fig. 4d). The results showed no significant changes in mRNA expression levels at SYN in the hippocampus across all three evaluated time points (Fig.

211 4e).

212 The increase of NAT10 proteins in SYN after memory formation could be due to
213 the upregulation of protein levels of NAT10 in HOM (i.e., the increase of de novo
214 protein synthesis). However, the protein levels of NAT10 were not altered in HOM of
215 mouse hippocampus on day 6 (Fig. 4f), suggesting that learning and memory did not
216 change the de novo protein synthesis of NAT10 in mouse hippocampus. To further
217 explore the distribution of NAT10 proteins in other subcellular fractions, we purified
218 the nucleus (N), cytoplasm (S2) and post-synaptic density (PSD) from the hippocampus
219 of control and learning mice on day 6, and analyzed the protein levels of NAT10 with
220 western blots (Fig. 4g). The nuclear fraction was enriched for histone but was depleted
221 of cytoplasmic protein α-tubulin or synaptic protein SYN1 and PSD95, and vice versa
222 for the S2 and PSD fraction (Extended Data Fig. S4a). The protein levels of NAT10 in
223 the nucleus of mouse hippocampus did not change after memory formation (Fig. 4h).
224 Strikingly, the NAT10 proteins were significantly reduced in the cytoplasm (S2 fraction)
225 but increased in the PSD fraction of mouse hippocampus after memory formation (Fig.
226 4i and 4j). These results suggest that NAT10 proteins might be relocated from
227 cytoplasm to synapses in mouse hippocampus after memory formation.

228 NAT10 belongs to the PCAF (p300/CBP-associated factor) subfamily of protein
229 acetyltransferase[40, 41]. Next, we aim to investigate whether learning and memory also
230 change protein levels of PCAF in the subcellular fractions of mouse hippocampus
231 (Extended Data Fig. S4b). The protein levels of PCAF did not change in HOM or
232 nucleus of the mouse hippocampus on day 6 after MWM training (Extended Data Fig.
233 S4c, d), indicating that learning and memory may not increase the de novo protein
234 synthesis of PCAF in mouse hippocampus. In contrast to NAT10, the protein levels of
235 PCAF in the cytoplasmic (S2) or PSD fractions of mouse hippocampus were not altered
236 after memory formation (Extended Data Fig. S4e, f). Altogether these results
237 demonstrate the specific increase of protein levels of NAT10 rather than PCAF in SYN
238 of mouse hippocampus after learning and memory.

239

240 **Downregulation of Nat10 in adult mouse hippocampus by cre/loxp**

241 In the following study, we used the cre/loxP strategy[42] to downregulate the expression
242 of Nat10 in adult mouse hippocampus. Given that Nat10 is mainly expressed in the
243 mature excitatory neurons of mouse hippocampus (Fig. 3), we used AAV that express a
244 cassette of EGFP-P2A-Cre or EGFP alone under the control of the human synapsin 1
245 (Syn1) promoter. Since dorsal hippocampus is more related with learning and memory
246 than ventral hippocampus[37-39], we injected AAV-EGFP or AAV-EGFP-P2A-Cre into the
247 dorsal hippocampus of Nat10$^{flox/flox}$ mice, which were named control and Nat10
248 conditional knockout (Nat10 cKO) mice, respectively (Fig. 5a). Both the control and
249 Nat10 cKO mice were trained in the MWM 3 weeks after AAV injection, and then the
250 hippocampal tissues were collected for biochemical assays on day 6 after probe tests
251 (Fig. 5a). The fluorescent protein EGFP was expressed mainly in the CA1-3 regions
252 and DG of mouse hippocampus 3 weeks after AAV injection (Fig. 5b), indicating the
253 successful infection of AAV. The protein levels of Nat10 were significantly reduced in
254 the dorsal hippocampus of Nat10 cKO mice, compared with controls (Fig. 5b and c),
255 verifying the knockdown efficiency of AAV. NAT10 was previously described as a
256 protein acetyltransferase against α-tubulin and histones[43-45]. In contrast to the dramatic
257 reduction observed in ac4C levels, immunoblotting with acetylation-specific antibodies
258 showed no significant change of protein acetylation in Nat10 cKO mouse hippocampus,
259 compared to controls (Fig. 5d-f), which suggests the redundancy of acetyltransferases
260 for α-tubulin and histones in mouse hippocampus. Likewise, the levels of ac4C rather
261 than m6A significantly decreased in Nat10 cKO mouse hippocampus, compared with
262 controls (Fig. 5g-h).
263

264 **Effects of NAT10-mediated ac4C modification on transcriptional activity**

265 To investigate Nat10-mediated ac4C modification in learning and memory, we recruited
266 Nat10$^{flox/flox}$ mice, divided into Cont and Nat10 cKO groups, for AAV injection. The
267 Cont group received a virus expressing EGFP, while the Nat10 cKO group was injected
268 with an AAV expressing EGFP in a Cre-dependent manner (Fig. 6a). The viral
269 injections were administered when the mice were six weeks old. At nine weeks, they
270 underwent Morris Water Maze (MWM) training and probe tests. After the probe test,

271 we analyzed hippocampal SYN by using low input acRIP-seq. The results revealed a
272 significantly lower ac4C peaks and ac4C mRNA in the hippocampal SYN of Nat10-
273 cko mice compared to the Cont group, while the number of mRNAs remained similar
274 between the two groups (Fig. 6b). Further analysis of mRNA samples from both Cont
275 and NAT10 cKO mice indicated a substantial reduction in ac4C-modified mRNA in the
276 NAT10 cKO group (Fig. 6c). Specifically, ac4C-modified mRNA decreased from 48.28%
277 in Cont group to 27.2% in NAT10 cKO group, indicating a significant loss of ac4C
278 modification following NAT10 knockout. We observed ac4C sites proximal to
279 translation start sites, with the majority of summits occurring within coding sequences
280 (CDS) (Fig3.e). The peak density of ac4C-modified mRNA in the CDS regions was
281 markedly lower in the NAT10 cKO group compared to Cont group (Fig. 6d). Sequence
282 motif analysis demonstrated a 'CXX' pattern in both groups (Fig. 6f). In the Cont group,
283 this sequence was present in 67.5% of peaks, but only in 18.65% of peaks in the NAT10
284 cKO group, suggesting an altered sequence preference following NAT10 knockout. The
285 cumulative distribution and box plot analysis fold enrichment of ac4C peaks (Fig. 6g)
286 and ac4C-mRNA (Fig. 6h) showed a significant reduction in the NAT10 cKO group.
287 This reduction suggests impaired modification efficiency in the absence of NAT10.
288 Notably, normalized mRNA counts showed no significant difference between the Cont
289 and NAT10 cKO groups (Fig. 6i), indicating that the observed effects on ac4C
290 modification are not due to changes in overall mRNA expression levels. The results
291 demonstrated a significant reduction in ac4C-modified mRNAs in the cKO group (Fig.
292 6j). We defined mRNAs whose fold enrichment (FE) levels of ac4C-modified mRNA
293 were downregulated in the cKO group compared to the Cont group as Nat10-mediated
294 mRNAs. Gene ontology analysis of the Nat10-mediated mRNAs revealed significant
295 enrichment in biological processes related to synaptic structure, synaptic function, and
296 cognitive processes such as learning and memory. This highlights the crucial role of
297 ac4C modification in maintaining synaptic integrity and cognitive functions (Fig.6 k).
298

299 **A representative NAT10-mediated N4-acetylcytidine Poly(A)-RNA for Arc**

300 Arc (activity-regulated cytoskeletal) gene is an immediate-early gene, and its mRNA

can be robustly induced by neural activities and targeted to stimulated synaptic area[46, 47]. Moreover, Arc plays critical roles in the consolidation of synaptic plasticity and spatial memory in the MWM[48], consistent with the finding that Arc is one of the core NAT10-mediatd gene in the PPI network of learning and memory (Fig. 7a).

We further investigated the ac4C peaks of Arc mRNA (abbreviated to ac4C-Arc thereafter) in SYN of control and learning mice at different time points after MWM learning. Although the levels of ac4C-Arc in SYN were low at basal conditions, the acetylation of Arc mRNA was robustly increased in SYN on day 6 rather than day 1 or 20 (Extended Data Fig. S5a, b, c and e). By contrast, the levels of ac4C-Arc in HOM were similar between control and learning mice on day 6 (Extended Data Fig. S5d). In addition, the Arc mRNA levels were not increased in SYN or HOM on day 6 (Extended Data Fig. S5f and 5g). In line with the change of ac4C, the protein levels of Arc were increased in SYN rather than HOM on day 6 (Extended Data Fig. 5h and 5i).

Regulation of ac4C and protein levels of Arc by Nat10 in SYN of learning mice

Given that Arc is a representative NAT10-mediated ac4C mRNA (Fig. 7a), we next address whether acetylation of Arc mRNA in SYN is regulated by NAT10. To this end, the ac4C and expression levels of Arc mRNA in SYN of Cont and Nat10 cKO mouse hippocampus were analyzed after MWM training and probe tests. Three samples (input, IgG-IP, acRIP) of SYN RNA were subjected to reverse transcription and quantitative polymerase chain reaction (RT-qPCR) for assessment of Arc mRNA levels (Fig. 7c). The results of RT-qPCR showed that Arc mRNA levels from the input were similar between Cont and Nat10 cKO groups (Fig. 7d). The Arc mRNA levels were very low when immunoprecipitated with IgG, compared with anti-ac4C antibodies (Fig. 7e), indicating the specificity of acRIP. Strikingly, the Arc mRNA levels were significantly reduced in the acRIP samples from Nat10 cKO group, compared with Cont group (Fig. 7f). These results demonstrate that Nat10 regulates ac4C rather than mRNA levels of Arc in SYN of learning mice.

Since ac4C modification in CDS of mRNA has been shown to promote translation efficiency[11, 12], we aim to study whether Nat10 regulates the protein levels of Arc in

SYN. The protein levels of Arc significantly decreased in SYN of Nat10 cKO mouse hippocampus after MWM training and probe tests, compared with Cont group (Fig. 7g), which suggests that Nat10 is important for Arc protein synthesis in SYN during learning and memory. By contrast, the protein levels of Arc in SYN were similar between the Cont and Nat10 cKO groups that were not trained in the MWM (Fig. 7h), which indicate that Nat10 may be dispensable for the Arc protein synthesis in SYN at basal conditions. Altogether these results demonstrate that Nat10 regulates ac4C and protein levels of Arc in SYN of mouse hippocampus during learning and memory. Altogether these results demonstrate that ac4C-Arc is upregulated in SYN after memory formation but returns to control levels after memory forgetting. Additionally, the reduction levels of ac4C-Arc in Nat10 cKO mice verify the notion that Arc is a representative Nat10-mediated mRNA (Fig. 7a).

Regulation of learning and memory by Nat10 in mouse hippocampus

In the following study, we investigate whether Nat10 in mouse hippocampus is important for learning and memory. Both Cont and Nat10 cKO groups were subjected to training in the MWM for 5 days, and the probe test was performed at day 6 (Fig. 8a). Both groups exhibited an overall decline in the latency to reach the platform at the early stage (day 1-2) of training (Fig. 8b). However, the Nat10 cKO group failed to improve performance during the late training stage (day 3-5), compared with Cont group (Fig. 8b). During the probe tests, the Cont and Nat10 cKO groups showed similar swimming speed and distance travelled (Fig. 8c and 8d). However, the time spent in the target area and the number of platform crossing were significantly reduced in Nat10 cKO group, compared with Cont (Fig. 8e-g). These results demonstrate that NAT10 in mouse hippocampus is important for spatial learning and memory.

The body and brain weight were similar between control and Nat10 cKO mice (Extended Data Fig. S6a, b). The number and intrinsic excitability of CA1 pyramidal neurons were also comparable between Cont and Nat10 cKO groups (Extended Data Fig. S6c, d). To address whether Nat10 regulates synaptic plasticity after learning and memory, we performed electrophysiology recording of the SC-CA1 synapses in the

361 Cont and Nat10 cKO groups with or without MWM training and probe tests (Fig. 8h).
362 Consistent with the previous report[49], the glutamatergic transmission at SC-CA1
363 synapses was significantly enhanced after MWM training and probe tests (Fig. 8i and
364 8j). The glutamatergic transmission at SC-CA1 synapses was similar between Cont and
365 Nat10 cKO groups without MWM training, which indicate that Nat10 may be
366 dispensable for the glutamatergic transmission at SC-CA1 synapses at basal conditions.
367 However, the glutamatergic transmission at SC-CA1 synapses was significantly
368 reduced in Nat10 cKO group after MWM training and probe tests, compared with Cont
369 (Fig. 8i and 8j). Altogether these results indicate that Nat10 specifically regulates
370 synaptic plasticity after learning and memory rather than basal glutamatergic
371 transmission in adult mouse hippocampus.
372

373 **Discussion**

374 In this study, we demonstrate the dynamic regulation of synaptic mRNA acetylation by
375 learning and memory in mouse hippocampus. Interestingly, the protein levels of NAT10
376 were also increased in the SYN after memory formation but returned to control levels
377 after forgetting. Likewise, the ac4C modification and protein levels of Arc, one
378 representative NAT10-mediated ac4C mRNA, in the SYN were regulated by NAT10 in
379 learning mice. Moreover, downregulation of NAT10 in mouse hippocampus impaired
380 synaptic plasticity and learning and memory.

381 Isolation of mRNA from total RNA samples was performed using an mRNA
382 enrichment kit based on base pairing between poly(A) residues in mRNA and
383 oligo(dT)25 covalently coupled to Dynabeads. Other cellular RNAs lacking a poly(A)
384 tail were expected to be washed away, although small amounts could potentially remain,
385 leading to an overestimation of the presence of ac4C in mRNA. UPLC-MS/MS was
386 used to determine the presence of ac4C in total RNA and mRNA from hippocampus.
387 This technique allowed the accurate detection of ac4C modifications directly within the
388 mRNA sequences. The purity of mRNA isolated using an mRNA purification kit was
389 evaluated by UPLC-MS/MS, which measured the relative amounts of 5S rRNA, 18S
390 rRNA, and 28S rRNA. The results indicated that mRNA was enriched in the isolated

samples, demonstrating that at least 90% of the ac4C signal observed in the mRNA analyses was representative of ac4C in mRNA rather than rRNA contamination. However, the possibility of tRNA contamination in the mRNA samples remains, although the combined use of dot blot and UPLC-MS/MS provides higher specificity in detecting ac4C modifications, significantly reducing the likelihood of such interference. Our results indicate that the level of ac4C modification in hippocampal mRNA is comparable to that of m6A. In addition, the level of ac4C stoichiometry in hippocampal mRNA is significantly higher than in most other tissues.

The dynamic regulation of protein acetylation in SYN by neural activities including learning and memory has been shown in our previous studies[50-53]. As compared to the well-characterized acetyltransferases and deacetylases for protein acetylation[54], the writer and eraser of mRNA acetylation are less well understood. The NAT10 acetyltransferase is the only known ac4C writer in the mammalian cells[16, 55]. Recently, the SIRT7 deacetylase has been shown to erase the ac4C modification of ribosomal RNA (rRNA) and small nucleolar RNA (snoRNA)[56, 57]. That said, the mechanisms underlying the deacetylation of mRNA need to be explored.

How the ac4C modification of mRNA is regulated by neural activities remains largely unknown. Our previous studies showed that overnight starvation downregulated the ac4C modification of tyrosine hydroxylase (TH) mRNA in the sympathetic nerve terminus that innervate the olfactory mucosa of mice, which reduced TH protein levels and dopamine synthesis in the mouse olfactory mucosa after overnight starvation[58]. In this study, we demonstrate that learning and memory regulate the dynamic change of ac4C modification of mRNA at synapses of mouse hippocampus. Altogether these two studies provide evidence that neural activities regulate acetylation of mRNA in a spatiotemporally specific manner.

The total protein levels of NAT10 in the HOM of mouse hippocampus were not altered after learning and memory. In contrast, the NAT10 proteins were increased in the SYN but reduced in the cytoplasm of mouse hippocampus after learning and memory. These results suggest a relocation of NAT10 from the cytoplasm to synapses during memory formation. Previous proteomic studies showed that NAT10 were

detected in the interactome with several motor proteins such as kinesin proteins[59], which raised the possibility that NAT10 might be transported by the motor proteins in hippocampal neurons during learning and memory.

Consistent with the previous studies showing that ac4C may promote mRNA translational efficiency[11, 12], we found that downregulation of NAT10 significantly reduced the protein rather than mRNA levels of Arc in the SYN after learning and memory. By contrast, downregulation of NAT10 did not lead to the reduction of Arc proteins in the SYN at basal conditions when the ac4C FE of Arc mRNA is pretty low. These results suggest that the ac4C modification of Arc mRNA needs to reach a certain high level to affect its protein synthesis in the SYN. On the other hand, ac4C may also increase the mRNA stability[11]. In this regard, it is possible that ac4C may enhance the stability of certain mRNAs in SYN after learning and memory.

Arc is an immediate-early gene, and its mRNA can be induced in several minutes by neural activities[46, 60-62]. However, studies from Arc knockout mice showed that Arc is essential for long-term memory that requires several days of training rather than short-term memory[48]. In line with the phenotypes of Nat10 cKO mice presented in this study, the Arc knockout mice showed deficits in the late phase of training and probe test in the MWM[48]. Interestingly, acetylation of Arc mRNA was increased in SYN on day 6 after MWM training when memories were consolidated, but not on day 1 after MWM training when memories were not formed. These dynamic changes of Arc mRNA acetylation in SYN well fit the function of Arc in learning and memory. New techniques for overexpression[63] and erasure of site-specifically acetylated mRNA need to be developed to study the function of mRNA acetylation. Nonetheless, the results presented here demonstrate the dynamic regulation and potentially important roles of mRNA acetylation in learning and memory.

References

1. Flavell, S.W. & Greenberg, M.E. Signaling mechanisms linking neuronal activity to gene expression and plasticity of the nervous system. *Annu. Rev. Neurosci.* **31**, 563-590 (2008).
2. Hafner, A.S., Donlin Asp, P.G., Leitch, B., Herzog, E. & Schuman, E.M. Local protein synthesis is a ubiquitous feature of neuronal pre-and postsynaptic compartments. *Science* **364**, eaau3644

(2019).
3. Monday, H.R., Kharod, S.C., Yoon, Y.J., Singer, R.H. & Castillo, P.E. Presynaptic FMRP and local protein synthesis support structural and functional plasticity of glutamatergic axon terminals. *Neuron* **110**, 2588-2606. e2586 (2022).
4. Ma, H. *et al.* γCaMKII shuttles Ca2+/CaM to the nucleus to trigger CREB phosphorylation and gene expression. *Cell* **159**, 281-294 (2014).
5. Fischer, A., Sananbenesi, F., Wang, X., Dobbin, M. & Tsai, L.-H. Recovery of learning and memory is associated with chromatin remodelling. *Nature* **447**, 178-182 (2007).
6. Levenson, J.M. *et al.* Regulation of histone acetylation during memory formation in the hippocampus. *Journal of Biological Chemistry* **279**, 40545-40559 (2004).
7. Kouzarides, T. Chromatin modifications and their function. *Cell* **128**, 693-705 (2007).
8. Merkurjev, D. *et al.* Synaptic N 6-methyladenosine (m6A) epitranscriptome reveals functional partitioning of localized transcripts. *Nature neuroscience* **21**, 1004-1014 (2018).
9. Boccaletto, P. *et al.* MODOMICS: a database of RNA modification pathways. 2017 update. *Nucleic acids research* **46**, D303-D307 (2018).
10. Stern, L. & LH, S. The role of the minor base N4-acetylcytidine in the function of the Escherichia coli noninitiator methionine transfer RNA. (1978).
11. Arango, D. *et al.* Acetylation of cytidine in mRNA promotes translation efficiency. *Cell* **175**, 1872-1886. e1824 (2018).
12. Arango, D. *et al.* Direct epitranscriptomic regulation of mammalian translation initiation through N4-acetylcytidine. *Molecular cell* **82**, 2797-2814. e2711 (2022).
13. Ito, S. *et al.* Human NAT10 is an ATP-dependent RNA acetyltransferase responsible for N4-acetylcytidine formation in 18 S ribosomal RNA (rRNA). *Journal of Biological Chemistry* **289**, 35724-35730 (2014).
14. Liu, Y. *et al.* N4-acetylcytidine-dependent GLMP mRNA stabilization by NAT10 promotes head and neck squamous cell carcinoma metastasis and remodels tumor microenvironment through MAPK/ERK signaling pathway. *Cell Death & Disease* **14**, 712 (2023).
15. Wang, G. *et al.* NAT10-mediated mRNA N4-acetylcytidine modification promotes bladder cancer progression. *Clinical and translational medicine* **12**, e738 (2022).
16. Hu, Z. *et al.* N-acetyltransferase NAT10 controls cell fates via connecting mRNA cytidine acetylation to chromatin signaling. *Science Advances* **10**, eadh9871 (2024).
17. Shi, J. *et al.* NAT10 is involved in cardiac remodeling through ac4C-mediated transcriptomic regulation. *Circulation Research* **133**, 989-1002 (2023).
18. Jiang, X. *et al.* Maternal NAT10 orchestrates oocyte meiotic cell-cycle progression and maturation in mice. *Nature Communications* **14**, 3729 (2023).
19. Zhang, M. *et al.* The cytidine N-acetyltransferase NAT10 participates in peripheral nerve injury-induced neuropathic pain by stabilizing SYT9 expression in primary sensory neurons. *Journal of Neuroscience* **43**, 3009-3027 (2023).
20. Xu, T. *et al.* Ac4C Enhances the Translation Efficiency of Vegfa mRNA and Mediates Central Sensitization in Spinal Dorsal Horn in Neuropathic Pain. *Advanced Science* **10**, 2303113 (2023).
21. Jarrard, L.E. On the role of the hippocampus in learning and memory in the rat. *Behavioral and neural biology* **60**, 9-26 (1993).
22. Moser, M.-B., Trommald, M. & Andersen, P. An increase in dendritic spine density on hippocampal CA1 pyramidal cells following spatial learning in adult rats suggests the formation

of new synapses. *Proceedings of the National Academy of Sciences* **91**, 12673-12675 (1994).

23. Morris, R. Developments of a water-maze procedure for studying spatial learning in the rat. *Journal of neuroscience methods* **11**, 47-60 (1984).

24. Guo, X.-F. *et al.* Elevation of N-acetyltransferase 10 in hippocampal neurons mediates depression-and anxiety-like behaviors. *Brain Research Bulletin* **185**, 91-98 (2022).

25. Sinclair, W.R. *et al.* Profiling cytidine acetylation with specific affinity and reactivity. *ACS chemical biology* **12**, 2922-2926 (2017).

26. Li, B. *et al.* FTO-dependent m6A modification of Plpp3 in circSCMH1-regulated vascular repair and functional recovery following stroke. *Nature Communications* **14**, 489 (2023).

27. Helm, M. & Motorin, Y. Detecting RNA modifications in the epitranscriptome: predict and validate. *Nat Rev Genet* **18**, 275-291 (2017).

28. Vorhees, C.V. & Williams, M.T. Morris water maze: procedures for assessing spatial and related forms of learning and memory. *Nature protocols* **1**, 848-858 (2006).

29. Hoz, L.d., Martin, S.J. & Morris, R.G.M. Forgetting, reminding, and remembering: the retrieval of lost spatial memory. *PLoS biology* **2**, e225 (2004).

30. Hobson, B.D. *et al.* Subcellular and regional localization of mRNA translation in midbrain dopamine neurons. *Cell reports* **38** (2022).

31. Arango, D., Sturgill, D. & Oberdoerffer, S. Immunoprecipitation and sequencing of acetylated RNA. *Bio-protocol* **9**, e3278-e3278 (2019).

32. Cajigas, I.J. *et al.* The local transcriptome in the synaptic neuropil revealed by deep sequencing and high-resolution imaging. *Neuron* **74**, 453-466 (2012).

33. Hafner, A.S., Donlin-Asp, P.G., Leitch, B., Herzog, E. & Schuman, E.M. Local protein synthesis is a ubiquitous feature of neuronal pre- and postsynaptic compartments. *Science* **364** (2019).

34. Niu, M. *et al.* Droplet-based transcriptome profiling of individual synapses. *Nat Biotechnol* **41**, 1332-1344 (2023).

35. Yu, Q. *et al.* Genetic labeling reveals temporal and spatial expression pattern of D2 dopamine receptor in rat forebrain. *Brain Structure and Function* **224**, 1035-1049 (2019).

36. Madisen, L. *et al.* A robust and high-throughput Cre reporting and characterization system for the whole mouse brain. *Nature neuroscience* **13**, 133-140 (2010).

37. Biane, J.S. *et al.* Neural dynamics underlying associative learning in the dorsal and ventral hippocampus. *Nature neuroscience* **26**, 798-809 (2023).

38. Fanselow, M.S. & Dong, H.-W. Are the dorsal and ventral hippocampus functionally distinct structures? *Neuron* **65**, 7-19 (2010).

39. Moser, E., Moser, M.-B. & Andersen, P. Spatial learning impairment parallels the magnitude of dorsal hippocampal lesions, but is hardly present following ventral lesions. *Journal of neuroscience* **13**, 3916-3925 (1993).

40. Lau, O.D. *et al.* p300/CBP-associated factor histone acetyltransferase processing of a peptide substrate: kinetic analysis of the catalytic mechanism. *Journal of Biological Chemistry* **275**, 21953-21959 (2000).

41. Dalhat, M.H., Altayb, H.N., Khan, M.I. & Choudhry, H. Structural insights of human N-acetyltransferase 10 and identification of its potential novel inhibitors. *Scientific reports* **11**, 6051 (2021).

42. Tsien, J.Z. *et al.* Subregion-and cell type–restricted gene knockout in mouse brain. *Cell* **87**, 1317-1326 (1996).

43. Shen, Q. *et al.* NAT10, a nucleolar protein, localizes to the midbody and regulates cytokinesis and acetylation of microtubules. *Experimental cell research* **315**, 1653-1667 (2009).
44. Lv, J. *et al.* Molecular cloning of a novel human gene encoding histone acetyltransferase-like protein involved in transcriptional activation of hTERT. *Biochemical and biophysical research communications* **311**, 506-513 (2003).
45. Liu, X. *et al.* NAT 10 regulates p53 activation through acetylating p53 at K120 and ubiquitinating Mdm2. *EMBO reports* **17**, 349-366 (2016).
46. Steward, O., Wallace, C.S., Lyford, G.L. & Worley, P.F. Synaptic activation causes the mRNA for the IEG Arc to localize selectively near activated postsynaptic sites on dendrites. *Neuron* **21**, 741-751 (1998).
47. Link, W. *et al.* Somatodendritic expression of an immediate early gene is regulated by synaptic activity. *Proceedings of the National Academy of Sciences* **92**, 5734-5738 (1995).
48. Plath, N. *et al.* Arc/Arg3. 1 is essential for the consolidation of synaptic plasticity and memories. *Neuron* **52**, 437-444 (2006).
49. Su, J. *et al.* Entorhinohippocampal cholecystokinin modulates spatial learning by facilitating neuroplasticity of hippocampal CA3-CA1 synapses. *Cell Reports* **42** (2023).
50. Zhang, H.-L. *et al.* SRC3 acetylates calmodulin in the mouse brain to regulate synaptic plasticity and fear learning. *Journal of Biological Chemistry* **297** (2021).
51. Zhang, H.-L. *et al.* Acetylation of calmodulin regulates synaptic plasticity and fear learning. *Journal of Biological Chemistry* **297** (2021).
52. Zhang, H.-L. *et al.* Steroid receptor coactivator 3 regulates synaptic plasticity and hippocampus-dependent memory. *Neuroscience Bulletin* **37**, 1645-1657 (2021).
53. Zhang, H.L. *et al.* HDAC9-mediated calmodulin deacetylation induces memory impairment in Alzheimer's disease. *CNS Neuroscience & Therapeutics* **30**, e14573 (2024).
54. Drazic, A., Myklebust, L.M., Ree, R. & Arnesen, T. The world of protein acetylation. *Biochimica et Biophysica Acta (BBA)-proteins and proteomics* **1864**, 1372-1401 (2016).
55. Cui, Z. *et al.* NAT10 promotes osteogenic differentiation of periodontal ligament stem cells by regulating VEGFA-mediated PI3K/AKT signaling pathway through ac4C modification. *Odontology* **111**, 870-882 (2023).
56. Xu, C., Zhang, J., Zhang, J. & Liu, B. SIRT7 is a deacetylase of N4-acetylcytidine on ribosomal RNA. *Genome Instability & Disease* **2**, 253-260 (2021).
57. Kudrin, P., Meierhofer, D., Vågbø, C.B. & Ørom, U.A.V. Nuclear RNA-acetylation can be erased by the deacetylase SIRT7. *BioRxiv*, 2021.2004. 2006.438707 (2021).
58. Zhou, H.-Q. *et al.* Olfactory regulation by dopamine and DRD2 receptor in the nose. *Proceedings of the National Academy of Sciences* **119**, e2118570119 (2022).
59. Rouillard, A.D. *et al.* The harmonizome: a collection of processed datasets gathered to serve and mine knowledge about genes and proteins. *Database* **2016** (2016).
60. Shepherd, J.D. & Bear, M.F. New views of Arc, a master regulator of synaptic plasticity. *Nature neuroscience* **14**, 279-284 (2011).
61. Lyford, G.L. *et al.* Arc, a growth factor and activity-regulated gene, encodes a novel cytoskeleton-associated protein that is enriched in neuronal dendrites. *Neuron* **14**, 433-445 (1995).
62. Na, Y. *et al.* Real-time imaging reveals properties of glutamate-induced Arc/Arg 3.1 translation in neuronal dendrites. *Neuron* **91**, 561-573 (2016).

63. Bartee, D., Nance, K.D. & Meier, J.L. Site-specific synthesis of N 4-acetylcytidine in RNA reveals physiological duplex stabilization. *Journal of the American Chemical Society* **144**, 3487-3496 (2022).
64. Thalalla Gamage, S., Sas-Chen, A., Schwartz, S. & Meier, J.L. Quantitative nucleotide resolution profiling of RNA cytidine acetylation by ac4C-seq. *Nature protocols* **16**, 2286-2307 (2021).
65. Heinz, S. *et al.* Simple combinations of lineage-determining transcription factors prime cis-regulatory elements required for macrophage and B cell identities. *Molecular cell* **38**, 576-589 (2010).
66. Wu, T. *et al.* clusterProfiler 4.0: A universal enrichment tool for interpreting omics data. *The innovation* **2** (2021).
67. Guca, E. *et al.* N6-methyladenosine in 5′ UTR does not promote translation initiation. *Molecular Cell* **84**, 584-595. e586 (2024).
68. Yin, D.-M. *et al.* Reversal of behavioral deficits and synaptic dysfunction in mice overexpressing neuregulin 1. *Neuron* **78**, 644-657 (2013).

Methods

Animals

Adult male mice were used in this study to eliminate the possible effects of the hormone cycle. For stereotaxic injection of AAV, six-week-old mice were used. For behavioral analysis, nine-week-old mice were used. For ac4C dot-blots, UPLC-MS/MS, acRIP-seq, and regular RNA-seq, mice aged between nine and ten weeks were used. For immunofluorescence, western blots and electrophysiology, ten-week-old mice were used. Animals were housed in rooms at 23°C and 50% humidity in a 12 h light/dark cycle and with food and water available ad libitum. Animal experimental procedures were approved by the Institutional Animal Care and Use Committee of East China Normal University.

Generation of Nat10$^{Cre/+}$ knockin mice

The mouse Nat 10 gene has 29 exons and the translational start codon (ATG) is localized in exon 2. We employed CRISPR/Cas9 technology in conjunction with homologous recombination to insert a Cre-WPRE-polyA expression cassette at the translational start codon of the Nat10 gene in C57BL/6J mice. The process commenced with the synthesis of Cas9 mRNA and a guide RNA (gRNA) targeting the start codon of Nat10, with the gRNA sequence being 5′-catcatgaatcggaagaaggtgg-3′. A donor vector was then constructed using In-Fusion cloning, containing 2.6 kb 5′ and 3′ homology arms flanking the Cre-WPRE-pA cassette, designed for Cre recombinase

expression, enhanced by the WPRE element and concluded with a polyadenylation signal. The cocktail of Cas9 mRNA, gRNA, and the donor vector was microinjected into fertilized C57BL/6J mouse embryos, leading to the birth of F0 generation mice. These mice were screened for the precise genomic integration of the cassette through PCR amplification and sequencing. Successful modifications were observed in F0 mice, which were subsequently bred with C57BL/6J mice to secure F1 progeny harboring the modification.

The resulting offspring were genotyped using PCR, with primers designed to detect the Cre within the Nat10 gene. The primers for genotyping wt Nat10 allele are as follows: forward: 5’tgtctttcctgtggtggtgt3’; reverse: 5’tgcgcactgaaaccctacaa3’. the primers for genotyping Nat10-cre allele are as follows: forward: 5’gaaatcatgcaggctggtgg3’; reverse: 5’aaagtcccggaaaggagctg3’. The PCR products for wt Nat10 and Nat10-Cre alleles were 392 and 393 bp, respectively.

Generation of floxed Nat10 mice

The generation of Nat10$^{flox/flox}$ mice involved targeted modification of exon 4 within the Nat10 gene, utilizing CRISPR/Cas9-mediated gene editing. Two guide RNAs (gRNAs) were specifically designed to target and flank exon 4, enabling a precise floxed modification. The sequences for these gRNAs were as follows: gRNA1: 5′-tcagcagaccactttaaagatgg-3′ and gRNA2: 5′-tgcctgacatagtaaggtctggg-3′. Both Cas9 mRNA and gRNAs were produced through in vitro transcription techniques. A donor vector for homologous recombination was constructed using In-Fusion cloning. This vector included a 3.0 kb 5′ homology arm, a 0.7 kb loxp-flanked region (flox), and a 3.0 kb 3′ homology arm to ensure accurate genomic insertion at the Nat10 locus. The mixture of Cas9 mRNA and the two gRNAs was injected into the cytoplasm of one-cell stage embryos. These embryos were subsequently implanted into pseudopregnant females and carried to term.

The resulting offspring were genotyped using PCR, with primers designed to detect the floxed exon 4 of Nat10 gene. The primers for genotyping the wt and floxed Nat10 allele are as follows: forward: 5’tgccgaggggatgtactcat3’; reverse: 5’agaaccccacgaactgtcct3’. The PCR products for wt Nat10 and floxed Nat10 allele were 302 and 356 bp, respectively.

Morris water maze (MWM)

The Morris Water Maze (MWM), a widely recognized method for assessing spatial learning and memory[28], was implemented with the following protocol: Mice were acclimated to the testing environment over a period of three days through 10-minute daily handling sessions. To aid navigation, visual cues were strategically positioned around the perimeter of the maze. To ensure consistency and minimize the impact of external variables, all experimental sessions were conducted simultaneously each day. During the core phase of the experiment, spanning five days, mice were subjected to four trials daily. In each trial, they were released from different quadrants into the maze, with the escape platform being fixed in the first quadrant. A trial was deemed complete when a mouse successfully located the platform within a 60-second timeframe. If unsuccessful, the mouse was gently guided to the platform at the 60-second mark. The probe test was performed on the sixth day, during which the platform was removed from the maze. Mice were then assessed based on their ability to navigate to the former location of the platform, serving as a measure of their retained spatial memory.

Chemical and reagents

All chemicals and reagents utilized in this study were of analytical grade. RNA was extracted using TRIzol® Reagent (15596-026, Invitrogen, Carlsbad, CA, USA) following the manufacturer's protocol. Chloroform and other general laboratory chemicals were obtained from Merck (109634, Darmstadt, Germany). The ACQUITY HSS T3 column (2.1×100 mm, 1.8 μm) for UPLC-MS/MS analysis was purchased from Waters Corporation (186008499, Milford, MA, USA). Phosphodiesterase was obtained from Sigma (P3243-1VL, St. Louis, MO, USA). S1 nuclease and alkaline phosphatase, used for RNA digestion, were obtained from Takara (2410A and 2250A). Hydroxylamine was from Aladdin Bio-Chem Technology Co., LTD (H164487). RNase Inhibitor, which is critical for preserving RNA integrity during manipulations, was purchased from New England Biolabs (M0314S, NEB, CA, USA). Methylene blue, which is used for nucleic acid visualization, was obtained from Abcam (M9140).

Subcellular fractionation

The procedure of subcellular fractionation was adapted from the methodologies in our previous studies[50, 51]. Mouse brain tissues were processed starting with homogenization in Buffer A, which consists of 0.32 M sucrose, 1 mM $MgCl_2$, 1 mM PMSF, and a protease inhibitor cocktail to ensure comprehensive cell lysis while preserving protein

integrity. The resultant homogenates were then filtered to remove cell debris and subsequently subjected to centrifugation at 500g for 5 minutes using a fixed-angle rotor. This step separates the homogenate into the pellet (P1) and supernatant (S1) fractions. The P1 fraction, containing primarily nuclei and unbroken cells, was further purified by resuspension in Buffer B (10 mM KCl, 1.5 mM $MgCl_2$, and 10 mM Tris-HCl at pH 7.4) followed by a repeat centrifugation under the same conditions to remove any remaining debris. The final pellet was resuspended in Buffer C (20 mM HEPES, pH 7.9, 25% glycerol, 1.5 mM $MgCl_2$, 1.4 M KCl, 0.2 mM EDTA, 0.2 mM PMSF, and 0.5 mM DTT), which is designed for nuclear protein extraction and incubated with agitation at 4 °C for 30 minutes to facilitate the release of nuclear proteins. A final centrifugation at 12,000g for 10 minutes was performed, and the supernatant, containing the nuclear protein fraction, was collected. The initial supernatant (S1), following the removal of P1, was further centrifuged at 10,000g for 10 minutes to partition it into the P2 fraction, which included the crude synaptosomes, and the cytosolic S2 fraction.

Western blot

Homogenates of hippocampus tissue were prepared in the RIPA buffer containing 50 mM Tris-HCl, pH 7.4, 150 mM NaCl, 2 mM EDTA, 1% sodium deoxycholate, 1% SDS, 1 mM PMSF, 50 mM sodium fluoride, 1 mM sodium vanadate, 1 mM DTT, and protease inhibitors cocktails. All the protein samples were boiled at 100 °C water bath for 10 minutes before western blot. Homogenates were resolved on SDS/PAGE and then transferred to nitrocellulose membranes, which were incubated in the TBS buffer (0.1% Tween-20 and 5% milk) for 1 hour at room temperature followed by incubation of primary antibodies overnight at 4 °C. After washing, the membranes were incubated with HRP-conjugated secondary antibody (goat-anti-rabbit, G-21234, 1:2000, Thermo Fisher) in the same TBS buffer for 2 hours at room temperature. Immunoreactive bands were visualized by ChemiDocTM XRS + Imaging System (BIO-RAD) using enhanced chemiluminescence (Pierce) and analyzed with Image J (NIH). The following primary antibodies were used: anti-H3 (1:1000, Cell Signaling, 9715), anti-SYN1 (1:1000, Cell Signaling, 2312), anti-α-tubulin (1:10000, Cell Signaling, 3873), rabbit anti-NAT10 (1:1000, Abcam, ab194297), anti-Acetyl-Histone H3 (1:1000, Cell Signaling, 9649), anti-Arc (1:1000, Proteintech, 66550-1-Ig), anti-PSD95 (1:1000, Cell Signaling, 3450),

anti-PCAF (1:1000, Cell Signaling, 3378), and rabbit anti-GAPDH (1:5000, Abways, ab0037).

Immunofluorescence

The mouse brains were fixed in 4% paraformaldehyde at room temperature for 1 hour and dehydrated in 20% sucrose at 4 ℃ overnight. Then the tissues were placed in an embedding mold and frozen in OCT media at 0 ℃. The embedded tissues were cut into slices with the thickness of 30 μm using a Leica microtome (CM3050S). The brain slices were permeabilized with 0.3% Triton-X 100 and 5% BSA in PBS and incubated with primary antibodies at 4 °C overnight. After washing with PBS for three times, samples were incubated with Alexa Fluor-594 secondary antibodies (goat-anti-rabbit, R37117; 1:1000, Thermo Fisher) for 2 hours at room temperature. Samples were mounted with Vectashield mounting medium (Vector Labs) and images were taken by Leica TCS SP8 confocal microscope. The following primary antibodies were used: rabbit anti-NeuN (1:1000, Abcam, ab177487), rabbit anti-Neurogranin (1:500, Abcam, ab217672). Unbiased stereology TissueFAX Plus ST (Tissue Gnostics, Vienna, Austria) was applied to count the number of NAT10-positive neurons. The detailed methods for cell number counting is available on the website (https://tissuegnostics.com/products/single-cell-analysis/tissuequest).

Detection of ac4C and m6A modifications by UPLC-MS/MS

The analysis of UPLC-MS/MS followed previous studies with some modification[11]. Briefly, the RNA samples starting with 2 μg, were digested into nucleosides using nuclease P1 and alkaline phosphatase at 37°C for 3 hours. The digested samples were then subjected to chloroform extraction, with the aqueous phase being utilized for UPLC-MS/MS analysis in an AB SCIEX QTRAP 6500+ system, featuring an ACQUITY HSS T3 column (2.1×100 mm, 1.8 μm). Chromatographic separation was achieved with a mobile phase gradient of 2 mM ammonium bicarbonate in ultrapure water (A) and methanol (B), starting with 95% A and transitioning to 5% A over 8 minutes. A calibration curve spanning 0.0005 to 1000 pmol standard samples facilitated the accurate quantification of the epitranscriptomic modifications.

ac4C and m6A dot-blot assay

The total RNA of mouse hippocampus was extracted with Trizol according to the manufacturer's instructions. The mRNA was then purified using the Dynabeads™ mRNA purification kit (61006, Thermo Fisher). The ac4C dot-blot was performed according to the previous study[19]. We used 0.5 μg of mRNA samples that fall in the linear range for each blot. In brief, the mRNA samples were denatured at 95 °C for 5 min using a heat block, immediately kept on ice for 1 min, loaded onto Amersham Hybond-N+ membrane and crosslinked with UV254 for 30 min. The membranes were blocked with 5% nonfat milk for 2 h at room temperature (RT), and incubated with the rabbit anti-m6A (1:2000, Synaptic System, #202003) or anti-ac4C antibody (1:500, Abcam, ab252215) at 4°C overnight. After wash with 0.05% PBST for three times, the membranes were incubated with the HRP-conjugated secondary antibody (goat-anti-rabbit, G-21234, 1:2000, Thermo Fisher) at RT for 2 h. The signals were visualized by ChemiDocTM XRS + Imaging System (BIO-RAD) using ECL and analyzed with Image J (NIH). RNA loading was verified by staining the membranes with 0.2% methylene blue. The intensity of each dot was normalized to total RNA.

Ultra-low input acRIP -seq

The Ultra-low input acRIP for SYN was performed following the previous studies with some modifications[11, 64]. Ultra-low input acRIP involves the removal of ribosomal RNA during the library preparation process following acRIP. This method is optimized for low amounts of RNA. Briefly, 1 μg of anti-ac4C antibody or control IgG (sc-2027, Santa Cruz) was coupled to Protein A/G Dynabeads (Share-Bio, SB-PR001) in PBS for 2 hours at RT. Then 30 μg of total RNA extracted from mouse hippocampus was fragmented using NEBNext® magnesium RNA fragmentation buffer at 94°C for 4 minutes. The fragmented RNA, which was approximately 300nt, was then immunoprecipitated with the anti-ac4C antibody or IgG-conjugated beads at 4°C after incubation with 100 μl acRIP buffer containing PBS, 0.05% Triton X-100, 0.1% BSA, 40 U murine RNase inhibitor (NEB, M0314S) for 4 hours. Following immunoprecipitation, the beads underwent three washes in acRIP buffer. RNA was then eluted through 100 μL RNase-free Proteinase K digestion buffer containing 50 mM Tris-HCl [pH 7.5], 75 mM NaCl, 6.25 mM EDTA, and 1% SDS for 1 hour at 37°C. RNA was extracted through phenol:chloroform [pH 4.5] and ethanol precipitation using 0.3M sodium acetate [pH 5.5] and 15 μg/mL linear acrylamide. The RNAs that were

immunoprecipitated along with 1% input were reverse transcribed using random hexamers, and then were subjected to second-generation sequencing. The RNA libraries for IP and input samples were constructed using the GenSeq Low Input Whole RNA Library Prep Kit from GenSeq Inc., following the manufacturer's instructions. This kit employs a strategy to eliminate ribosomal cDNA by using probes specific to mammalian rRNA after reverse transcription and amplification. The libraries were qualified using the Agilent 2100 bioanalyzer from Agilent and then sequenced using the NovaSeq 6000 system (Illumina). The sequencing data quality was assessed using Q30. Low-quality reads and 3' adaptors were removed using cutadapt software (v1.9.3). The high-quality and clean reads were aligned to the reference genome using Hisat2 software (v2.0.4). Raw counts were obtained using HTSeq software (v0.9.1), and normalization was performed using edgeR (v3.16.5). The gene expression level was quantified in terms of FPKM (Fragments Per Kilobase of transcript per Million mapped reads). The differentially expressed genes (DEGs) were identified based on p value < 0.05 and fold change ≥2.

Quantification and statistical analysis of ac4C epitranscriptome

Identification of ac4C peaks and position analysis of acetylated sites

After RNA integrity control, acRIP enrichment control, and library quality control, the raw reads were subjected to quality control using Q30 and Fast QC. Subsequently, 3’ adaptor-trimming and low-quality read were removed by cutadapt software (v1.9.3) to get a clean read. A post-alignment filter removed alignments to mitochondrial DNA (chrM) and non-concordant mate pairs. After that, clean reads were mapped to the mouse genome (mm10) with Hisat2 software (v2.04).

To identify acetylated sites, we analyzed the clean reads' enrichment in acRIP and input samples. We used MACS software (v1.4.2) to identify regions where significant enrichment of clean reads occurred in acRIP samples, with parameters selected to optimize performance with transcript mapped reads (i.e., turning off the shifting model and local lambda, and using tsize 150 as the sequencing read length). Input samples were used as controls for peak calling. The identified regions were designated as acetylated sites, and ac4C peaks with a bed or bam format were generated. These peaks can be visualized on the UCSC genome browser (https://genome.ucsc.edu/cgi-bin/hgGateway) using IGV (http://www.igv.org/).

To ensure data reliability, we established strict screening criteria in the peak calling process. First, we calibrated using non-specific IgG binding peaks and kept only those with no coordinate overlap. Second, we selected only the peaks on the protein-encoding exon for subsequent analysis. Lastly, we screened the peaks using the following criteria: Adjusted $p < 0.05$ and a Fold Enrichment (FE) > 2. A significance threshold of FDR adjusted $p < 0.05$ was classified as statistically significant differential expression. The relative representation of peaks, we classify fold enrichment with summits in >2 feature as "ambiguous," and exclude them from analysis. The FE was calculated as the difference of acRIP divided by the input.

$$FE = \frac{acRIP}{Input}$$

Sequence motif analysis

Sequence motifs were identified using HOMER[65] and visualized using ggseqlogo package from R software. HOMER identifies motifs that are specifically enriched on learning set of sequences relative to control (e.g., peaks upstream and downstream sequences relative to the entire genome sequence) based primarily on the principle of ZOOPS scoring with hypergeometric enrichment.

Gene ontology and functional category analysis

Gene ontology (GO) analysis to detect enrichment for GO terms in differential acetylation genes in R using the clusterProfiler[66], and the possible roles of these differential acetylation genes were annotated according to MF, BP and CC. GO terms with a false-discovery rate adjusted P-value of < 0.05 were visualized using R scripts to plot. The R package clusterProfiler to visualize the genes composing KEGG pathways, and P-value < 0.05 was used as the threshold of significant enrichment.

Analysis of ac4C fold enrichment (FE) for individual mRNAs

The fold enrichment of ac4C-mRNA was reflected by the cumulative value of multiple ac4C peaks from one particular mRNA molecule. Aggregating the cumulative sum of these peaks offers a more comprehensive overview of the total abundance of ac4C modifications across the mRNA molecule, avoiding the narrow focus on a potentially non-representative, single maximum modification site, similar with the previous study of m6A[67]. Additionally, in instances where ac4C modifications on mRNA are more dispersed or present in low abundance, a single prominent peak may not be observable; instead, multiple low-abundance peaks might emerge. In such scenarios, the accumulation of multiple peaks can enhance detection sensitivity, better capture

dynamic changes, and mitigate biases inherent in individual experiments.

This study showed that ac4C mainly occurred in mRNA in mouse hippocampus. In addition, previous studied indicated that the influence of different ac4C peaks within the CDS on translation efficiency is consistent[11, 12]. The following quantification index was used to calculate the ac4C levels of individual mRNA:

$$FE\ of\ ac4C = \Sigma peak\ (1 + 2 + 3 \ldots \ldots + n)$$

Analysis of ac4C fold change (FC) for individual mRNAs

The fold change of ac4C-mRNA is representative of the degree of change in the overall acetylation level of mRNA in the learning group (L) compared with the control group (C). To prevent a value of 0 in the denominator in the FC calculation, we added 1 to the FE of ac4C. The FC of ac4C-mRNA was calculated using the following quantification index:

$$FC\ of\ ac4C = \frac{(FE\ of\ ac4C + 1)\ in\ L}{(FE\ of\ ac4C + 1)\ in\ C}$$

Analysis of ac4C clusters regulated by learning and memory

By using Mfuzz to analyze time-series ac4C levels, the fuzzy C-mean clustering algorithm can effectively deal with the common noise and uncertainty in biological data. To study the dynamics of ac4C mRNA during learning memory by analyzing and comparing ac4C levels differences between control and learning mice at three time points, we have theoretically and numerically shown that if there is a cluster of genes, satisfying the following three criteria from the observed data:

(1) Standard deviations (SD) of genes (ac4C expression levels) in this cluster are increased markedly.

(2) Pearson correlation coefficients (PCC) of ac4C-mRNA in this cluster are increased significantly.

(3) PCC between ac4C-mRNA in this cluster and others are decreased significantly.

The PCC is used to measure the correlation between ac4C-mRNA and its cluster. PCC values range from 0 to 1, with higher values indicating stronger correlation between ac4C-mRNA and clusters.

Analysis of PPI network

The STRING (https://string-db.org/) (version 12.0) knowledge base was used to create a protein-protein interaction (PPI) network of genes enriched in the top 10 molecular function (MF) pathways for LISA genes. The objective was to examine the functional and physical connections between LISA genes. The PPI network of LISA genes was

generated with a confidence score of 0.7 and visualized using Cytoscape (version 3.10.1). Molecular Complex Detection (MCODE) (v2.0.3) algorithm was employed to identify the components of the densely connected network.

The following software and algorithms were used for the quantification and statistical analysis of ac4C epitranscriptome.

Software and algorithms, application, authors		
R v4.3.2	Statistical computing and graphics.	R Core Team. R Foundation for Statistical Computing 2023.
Python v3.11	Object-oriented programming language.	Van R et al. CreateSpace 2009.
ggplot2	Creating graphics, based on The Grammar of Graphics.	Hadley W et al, Springer-Verlag New York 2016.
ggseqlogo	Generating publication-ready sequence logos using ggplot2.	Wagih et al. Bioinformatics 2018.
tidyverse	Collection of R packages designed for data science.	Wickham et al. Journal of Open Source Software 2019.
mfuzz	Noise-robust clustering of gene expression time-series data.	Kumar L et al. Bioinformatics 2007.
ComplexHeatmap	Arrange multiple heatmaps and supports annotation graphics.	Gu Z et al. Bioinformatics 2016.
HOMER v4.11	Motif Discovery and gene sequencing analysis.	Heinz S et al. Mol Cell 2010.
bedtools	Compare large sets of genomic features.	Aaron Q et al. Bioinformatics 2010.
cutadapt v1.9.3	Remove sequencing data adaptor.	Martin M. EMBnet 2011.
Hisat2 v2.04	Mapping sequencing reads to a single reference genome.	Zhang Y et al. Genome Research 2021.
MACS v1.4.2	Identifying transcript factor binding sites.	Yong Z et al. Genome Biology 2008.
Pandas v2.1.4	Cleaning data.	The pandas development team. Zenodo 2020.
IGV	Interactive genome visualization	James T et al. Bioinformatics

	application.	2023.
HTSeq (v0.9.1)	Analysing high-throughput sequencing data.	Simon A et al. Bioinformatics 2014.
edgeR (v3.16.5)	Empirical analysis of digital gene expression data.	McCarthy DJ et al. Nucleic Acids Research 2012.

RT-qPCR

The cDNA was obtained through reverse transcription using the HiScript III RT SuperMix for qPCR kit (Vazyme, R323-01), followed by amplification using the ChamQ Universal SYBR qPCR Master Mix kit (Vazyme, Q711-02). Gene expression levels measured with RT-PCR were normalized to Gapdh. The primers used in qPCR for this study were as follows: Arc-forward, 5'ggagggaggtcttctaccgtc3'; Arc-reverse 5'cccccacacctacagagaca3'; Gapdh-forward, 5'gggtgtgaaccacgagaaat3'; Gapdh-reverse 5'actgtggtcatgagcccttc3'.

Stereotaxic injection of AAV into mouse hippocampus

AAV2/9-Syn1-EGFP and AAV2/9-Syn1-EGFP-P2A-Cre were generated by Hanbio Technology (Shanghai) Corp., Ltd., with a titer of 10^{12}/μl. We injected 0.3 μl AAV into each side of the mouse hippocampus. Six-week-old Nat10$^{flox/flox}$ mice received an intraperitoneal injection of alphaxalone at a dosage of 40 mg/kg for anesthesia and then were immobilized in a stereotaxic frame provided by RWD Life Science. Similarly, AAV2/9-CAG-DIO-EGFP, generated by Hanbio Technology (Shanghai) Corp., Ltd., with a titer of 10^{12}/μl, was injected into the hippocampus of seven-week-old Nat10$^{Cre/+}$ mice. The AAVs were delivered into mouse hippocampus through a Stoelting stereotaxic injector at a flow rate of 0.1 μl/min. The precise coordinates for the stereotaxic injection were set to anteroposterior (AP) −2.3 mm, dorsoventral (DV) −1.8 mm, and mediolateral (ML)±1.75 mm, relative to the Bregma.

Electrophysiological recording

The electrophysiological recording in mouse hippocampus was performed following the protocols in our previous study[68]. To investigate the glutamatergic transmission at SC-CA1 synapses, we recorded the input/output (I/O) curves of AMPA receptor-

919 medicated field excitatory postsynaptic potentials (fEPSP) at SC-CA1 synapses. Ten-
920 week-old mice were anesthetized and decapitated. The mouse brains were rapidly
921 removed and placed in ice-cold and oxygenated (95% O2 and 5% CO2) artificial
922 cerebrospinal fluid (aCSF) containing (in mM): 124 NaCl, 3 KCl, 26 NaHCO3, 1.25
923 NaH_2PO_4, 1 $MgSO_4$, 10 D-glucose, and 2 $CaCl_2$. The hippocampal slices were cut at a
924 thickness of 400 μm using a vibratome (Leica, VT1000s) and were placed in the
925 oxygenated aCSF under room temperature for 1 h before recording. The hippocampal
926 slices were placed in a recording chamber continuously superfused with prewarmed (32
927 ± 1°C) aCSF at a rate of 3 ml/min. fEPSPs were evoked (0.033 Hz, 0.1 ms current
928 pulses) in the CA1 stratum radiatum by stimulating Schaffer collateral (SC) with a two-
929 concentrical bipolar stimulating electrode (FHC) and recorded in current clamp by a
930 HEKAEPC 10 (HEKA Elektronik) amplifier with aCSF-filled glass pipettes (1–3 MΩ).
931 For building up an I/O curve, fEPSPs were evoked by a serial of incremental intensities
932 (0.02–0.2 mA in 0.02 mA increments, 100 μs in duration, at 0.033 Hz). All data were
933 acquired at a 10 kHz sampling rate of using PATCHMASTER version 2 x 90.1 software
934 (HEKA Elektronik) and filtered offline at 1 kHz.
935 The voltage clamp was used to analyze the intrinsic excitability of CA1 pyramidal
936 neurons. Neurons were held at -70 mV and injected with various currents (duration:
937 500 ms; increments: ±20 pA; range: -100 to 400 pA; interval: 10 s). The input-output
938 relationship was determined by plotting the amplitude of current injection against the
939 number of action potentials.
940
941 **Generation and use of the ac4C website**
942 The ac4Catlas website was constructed using HTML (a scripting language for front-
943 end development), PHP (a scripting language for backend development), and MySQL
944 (a structured query language for data operation). All the website codes were deployed
945 in a Linux server equipped with Centos environment. The raw data, processed data and
946 annotated files were stored in "Data Downloads" section. JBrowse (https://jbrowse.org)
947 was integrated to visualize the ac4C epitranscriptomic data on genomic regions of
948 interest. Briefly, ac4Catlas provides user-friendly interactive interfaces which allow

researchers to freely browse and perform extended operations, such as searching, comparing, and downloading. Besides, the browse module stores detailed information of samples and corresponding datasets as well as ac4C levels of mRNA and differentially acetylated regions between groups.

Statistical analysis

The cumulative distribution was analyzed by Kolmogorov-Smirnov test in R. The statistical analysis of percentage of ac4C summits occurring within CDS or UTRs was performed by chi-square test in R. Except the above-mentioned bioinformatic data, all other data were shown as mean ± SEM unless otherwise mentioned. The sample size justification was based on the previous studies and met the requirement of statistics power. For normally distributed data with 1 experimental variable, statistical analyses were performed by parametric analysis: unpaired (two-tailed) student's t-test for two groups and one-way ANOVA with the Tukey's multiple-comparison test for 3 groups. Data with >1 experimental variable were evaluated by two-way ANOVA, with post hoc Tukey, Dunnett or Sidak's multiple-comparison tests. All these statistical analyses were performed by the software of GraphPad Prism 11. Statistically significant difference was indicated as follows: **** $P < 0.0001$, *** $P < 0.001$, ** $P < 0.01$ and * $P < 0.05$.

Acknowledgements

We thank CloudSeq Inc. (Shanghai, China) for providing us with technical support on acRIP-seq and regular RNA-seq. This work was supported by STI2030-Major Projects (Grant No. 2021ZD0202500) and the National Natural Science Foundation of China (Grant No. 32300560), and the Fundamental Research Funds for the Central Universities (Grant No. YBNLTS2022-011).

Author contributions

H.-Q.Z., F.-Y.D. and H.J. performed biochemical and behavioral analysis, H.-Q.Z., J.-W.Z., and Z.Z. analyzed the data, W.-P.L. and Y.-Y.D. performed electrophysiology. D.-H.W. provided reagents. D.-S.C. generated the ac4C website, D.-M.Y. conceived the

idea, supervised the work and wrote the paper. All authors approved the final version of the manuscript.

Competing interests

The authors declare no competing interests.

Data and materials availability

All data are available in the main text, supplementary or source data files. The original data of acRIP-seq and regular RNA-seq is accessible via the website (http://ac4Catlas.com/) or GEO database. The source data files are provided with the paper, which contain high-resolution figures, uncropped western blot images, and original statistical data. All unique materials used are readily available from the corresponding author upon reasonable requests.

Code availability

Custom code used in this paper is available at https://github.com/YinDMlab/ac4CRIP-seq-analysis.

Figures and Legends

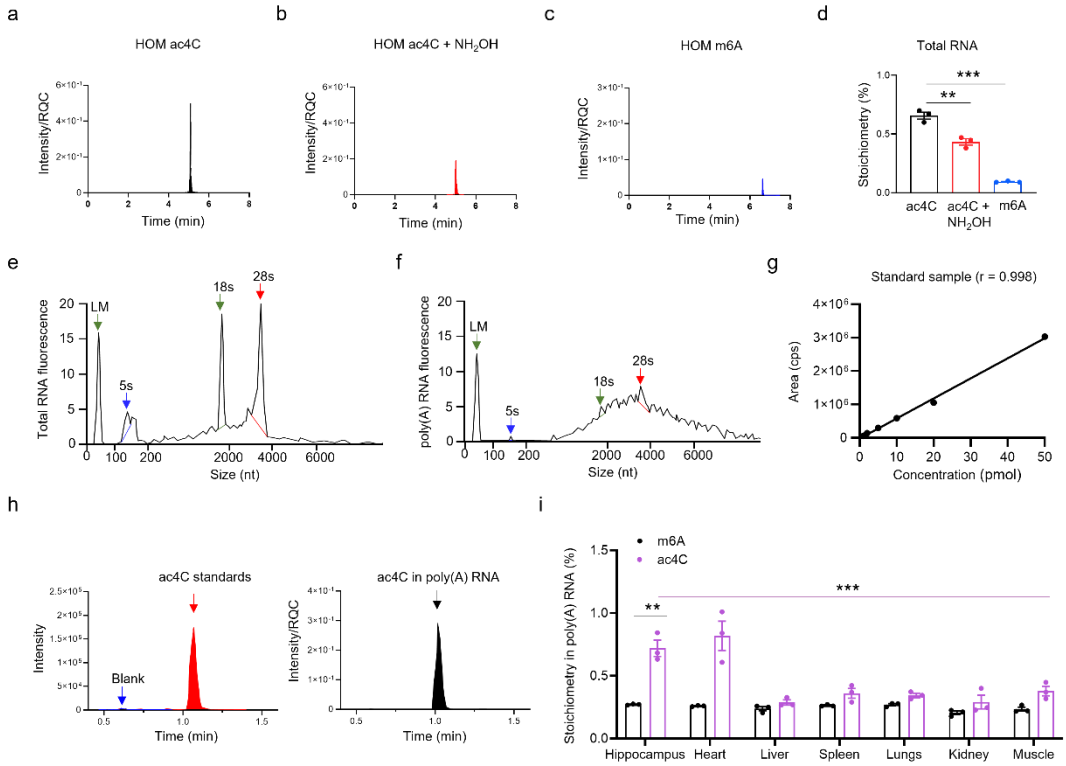

Fig. 1 Demonstrating the presence of ac4C in mouse hippocampal poly(A) RNA. **a-b**, Peaks of ac4C in 2 μg HOM from mouse hippocampal tissue (**a**) and NH_2OH-treated hippocampal tissue (**b**) that were identified by UPLC-MS/MS. The x-axis corresponds to the elapsed time, while the y-axis denotes the intensity relative to the quality control (RQC). **c**, Peak of m6A in 2 μg HOM from mouse hippocampal tissue that was identified by UPLC-MS/MS. The x-axis corresponds to the elapsed time, while the y-axis denotes the intensity relative to the quality control (RQC). **d**, The stoichiometry levels of ac4C were higher than m6A in HOM from mouse hippocampus, but were reduced after NH_2OH treatment. Data in panel a-c were quantified and presented as mean ± SEM. n = 3 biological replicates at each condition, ** P = 0.005, *** P < 0.001, two-tailed t-test. **e-f**, Poly(A) RNA was isolated using mRNA purification kit and purity verified through size distribution in bioanalyzer profiling. **g**, Standard curve for ac4C quantification using UPLC-MS/MS. The standard samples, prepared at varying concentrations of ac4C (1 pmol, 2 pmol, 5 pmol, 10 pmol, 20 pmol, and 50 pmol), were analyzed to generate a calibration curve. The x-axis represents the concentration of the ac4C standard samples (pmol), and the y-axis represents the corresponding UPLC-MS/MS signal area (cps). The linear regression analysis yielded

a correlation coefficient (r) of 0.998, indicating a strong linear relationship between concentration and signal response, thus validating the sensitivity and accuracy of the UPLC-MS/MS method for ac4C quantification in mRNA. **h**, Chromatograms are representative of UPLC-MS/MS analysis performed on poly(A) RNA isolated from the hippocampus of wild-type mice. Blank samples and ac4C standards were included as controls to ensure the accuracy and reliability of the measurements. **i**, Stoichiometry of m6A and ac4C modifications in poly(A) RNA from various mouse tissues. The bar graph shows the percentage of m6A (black) and ac4C (purple) modifications in poly(A) RNA isolated from the hippocampus, heart, liver, spleen, lungs, kidney, and muscle of wild-type mice. n = 3 biological replicates at each condition, ** P = 0.0022, two-tailed t-test. *** P < 0.0001, one-way ANOVA was performed to assess the differences in ac4C levels across different tissues.

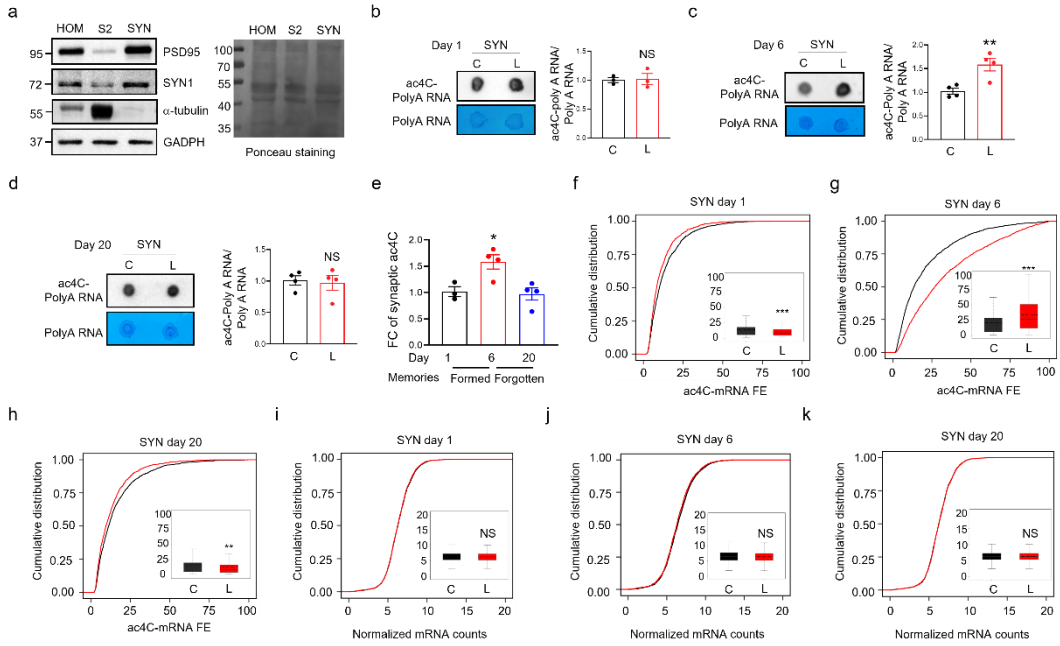

Fig. 2 Increased mRNA acetylation in SYN of mouse hippocampus after learning and memory. a, The purified synaptosomes (SYN) of mouse hippocampus expressed high levels of PSD95 and synapsin 1 (SYN1), two synaptic protein markers, but very low levels of β-tubulin, a cytoplasmic protein marker. The HOM, S2 and SYN of mouse hippocampus were subjected to western blots with the indicated antibodies. Left panel, representative images of western blots; right panel, Ponceau staining to show equal protein loading. **b**, Acetylation of mRNA was not altered in SYN of mouse

hippocampus on day 1 after MWM training when memories were not formed. The SYN mRNA samples of control and learning mice on day 1 were subjected to ac4C dot-blots and methylene blue staining. Left, the representative images of ac4C dot-blots and methylene blue staining; right, quantification data. n = 3 biological replicates for day 1, NS, not significant, two-tailed t-test. Data were normalized by controls. **c**, Acetylation of mRNA was increased in SYN of mouse hippocampus after memory formation. The SYN mRNA samples of control and learning mice on day 6 were subjected to ac4C dot-blots and methylene blue staining. Left, the representative images of ac4C dot-blots and methylene blue staining; right, quantification data. n = 4 biological replicates at each condition, ** P = 0.0093, two-tailed t-test. Data were normalized by controls. **d**, Acetylation of mRNA was not altered in SYN of mouse hippocampus on day 20 when memories had been forgotten. The SYN mRNA samples of control and learning mice on day 20 were subjected to ac4C dot-blots and methylene blue staining. Left, the representative images of ac4C dot-blots and methylene blue staining; right, quantification data. n = 4 biological replicates for day 20, NS, not significant, two-tailed t-test. Data were normalized by controls. **e**, Acetylation of mRNA in SYN was increased during memory formation but returned to normal levels after forgetting. Shown are FC of ac4C on day 1, 6 and 20 after MWM training. * P = 0.0112, one-way-ANOVA. C, control; L, learning; FC, Fold Change. **f-h**, Acetylation levels were increased after memory formation but returned to normal after forgetting in SYN of mouse hippocampus. Shown are cumulative distribution curves of ac4C for SYN in control (C) and learning (L) mice on day 1 (f), 6 (g), and 20 (h). The ac4C FE of each group was quantified in the quartile boxplots, where the solid line in the box is the median and the dashed line is the mean, where the maximum and minimum values are identified. *** P = 1.885e-06 for day 1, *** P < 2.2e-16 for day 6, ** P = 0.001738 for day 20, Kolmogorov-Smirnov test. **i-k**, mRNA levels were not significantly changed in SYN of mouse hippocampus during learning and memory. Shown are cumulative distribution curves of mRNA counts for SYN in C and L mice on day 1 (i), 6 (j) and 20 (k). The normalized mRNA counts of each group were quantified in the quartile boxplots. NS, not significant, Kolmogorov-Smirnov test.

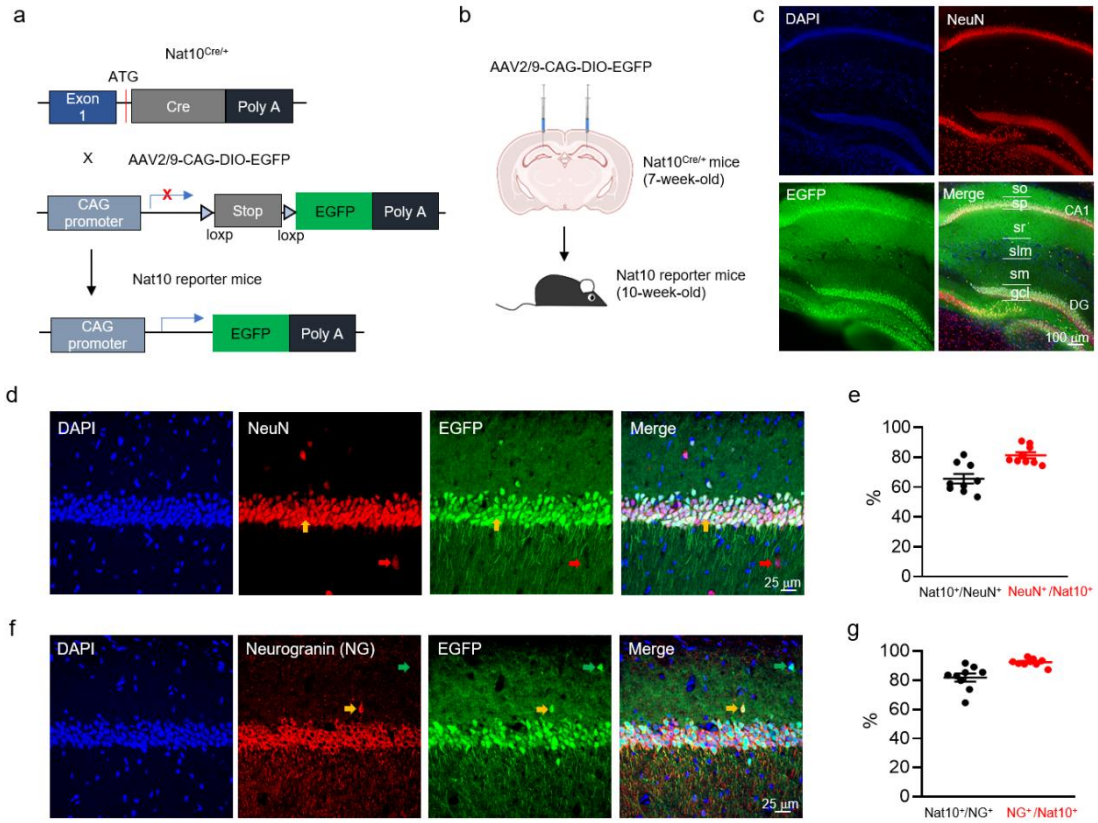

Fig. 3 Expression of Nat10 in neurons of mouse hippocampus. a, Schematic diagram of the gene targeting strategy to generate Nat10 reporter mice. **b**, Experimental design. Cre-reporting AAV was injected into the dorsal hippocampus of 7-week-old Nat10$^{Cre/+}$ mice. Three weeks after AAV injection, the fluorescent protein EGFP was analyzed in the Nat10 reporter mice. **c**, Co-localization of EGFP with NeuN in the hippocampus of Nat10 reporter mice. The hippocampal slices from Nat10 reporter mice were immunostained with anti-NeuN antibodies. so, stratum oriens; sp, stratum pyramidale; sr, stratum radiatum; slm, stratum lacunosum-moleculare; sm, stratum moleculare; gcl, granule cell layer; DG, dentate gyrus. Scale bar, 100 μm. **d**, Co-localization of EGFP and NeuN in the CA1 region of Nat10 reporter mice. The hippocampal slices from Nat10 reporter mice were immunostained with anti-NeuN antibodies. The yellow arrow indicates a neuron expressing Nat10, while the red arrow represents a neuron not expressing Nat10. Scale bar, 25 μm. **e**, Quantification of the percentage of NeuN-positive cells expressing Nat10 (Nat10^{+} / NeuN^{+} = 65.61 ± 3.245%) and the percentage of Nat10-positive cells expressing NeuN (NeuN^{+} / Nat10^{+} = 81.31 ± 2.029%). n = 9 slices from 3 mice. **f**, Co-localization of EGFP and Neurogranin (NG) in the CA1 region

of Nat10 reporter mice. The hippocampal slices from Nat10 reporter mice were immunostained with anti-NG antibodies. The yellow arrow indicates an excitatory pyramidal neuron expressing Nat10, while the green arrow represents a non- pyramidal cell expressing Nat10. Scale bar, 25 μm. **g**, Quantification of the percentage of NG-positive cells expressing Nat10 ($Nat10^{+}$ / NG^{+} = 81.87 ± 2.765%) and the percentage of Nat10-positive cells expressing NG (NG^{+} / $Nat10^{+}$ = 92.4 ± 0.852%). n = 9 slices from 3 mice.

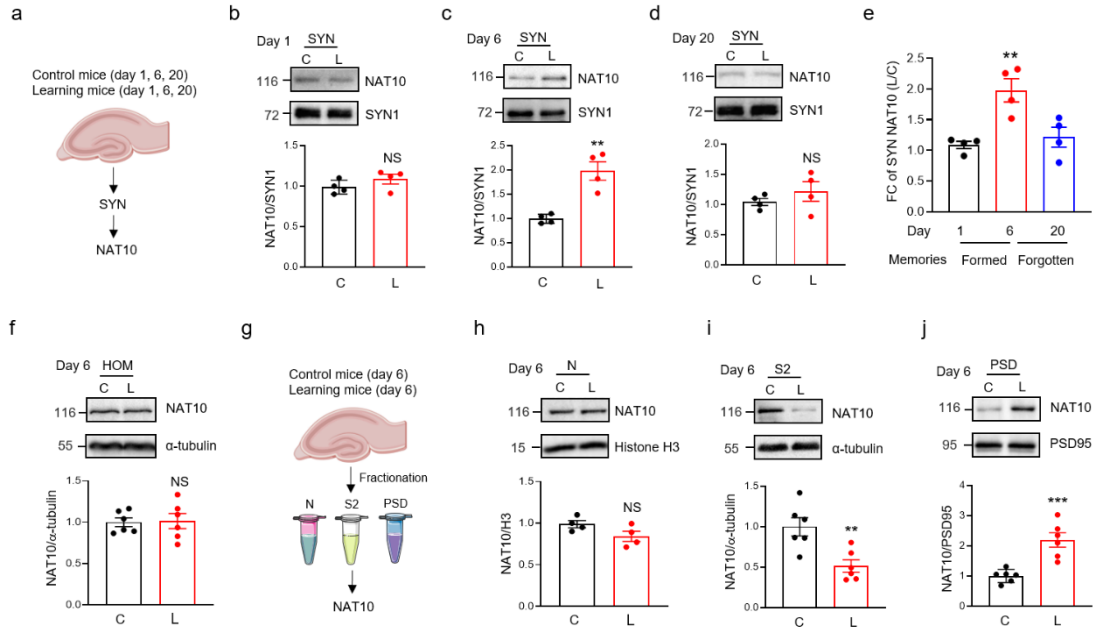

Fig. 4 Increased NAT10 proteins in SYN of mouse hippocampus after learning and memory. a, Experimental design. Proteins were extracted from SYN of control and learning mouse hippocampus on day 1, 6, and 20 after MWM training, and then NAT10 protein levels were assessed by western blots. **b-e**, Protein levels of NAT10 were increased in SYN after memory formation but returned to normal levels after forgetting. The SYN protein samples from control and learning mice on day 1 (**b**), 6 (**c**), and 20 (**d**) after MWM training were subjected to western blots with the indicated antibodies. Top, representative western blot images; bottom, quantification data. n = 4 biological replicates at each condition, NS, not significant, ** P = 0.0023, two-tailed t-test. Data were normalized by controls. **e**, FC of SYN NAT10 proteins on day 1, 6, and 20 after MWM training. n = 4 biological replicates at each condition, ** P = 0.0043, one-way-ANOVA. **f**, Protein levels of NAT10 were not altered in HOM after memory formation.

The HOM protein samples from control and learning mice on day 6 after MWM training were subjected to western blots with the indicated antibodies. Top, representative western blot images; bottom, quantification data. n = 6 biological replicates at each condition, NS, not significant, two-tailed t-test. Data were normalized by controls. **g**, Experimental design. Proteins were extracted from nucleus (N), cytoplasm (S2), and postsynaptic density (PSD) of control and learning mouse hippocampus on day 6 after MWM training, and then NAT10 protein levels were assessed by western blots. **h**, Protein levels of NAT10 were not altered in the nuclear fraction of mouse hippocampus after memory formation. The samples of nuclear proteins from control and learning mice on day 6 after MWM training were subjected to western blots with the indicated antibodies. Top, representative western blot images; bottom, quantification data. n = 4 biological replicates at each condition, NS, not significant, two-tailed t-test. Data were normalized by controls. **i-j**, Protein levels of NAT10 were significantly reduced in the S2 fraction (**i**) but increased in the PSD fraction (**j**) of mouse hippocampus after memory formation. The samples of cytoplasmic and PSD proteins from control and learning mice on day 6 after MWM training were subjected to western blots with the indicated antibodies. Top, representative western blot images; bottom, quantification data. n = 6 biological replicates at each condition, ** P = 0.0052 (i), *** P = 0.0008 (j), two-tailed t-test. Data were normalized by controls. C, control; L, learning.

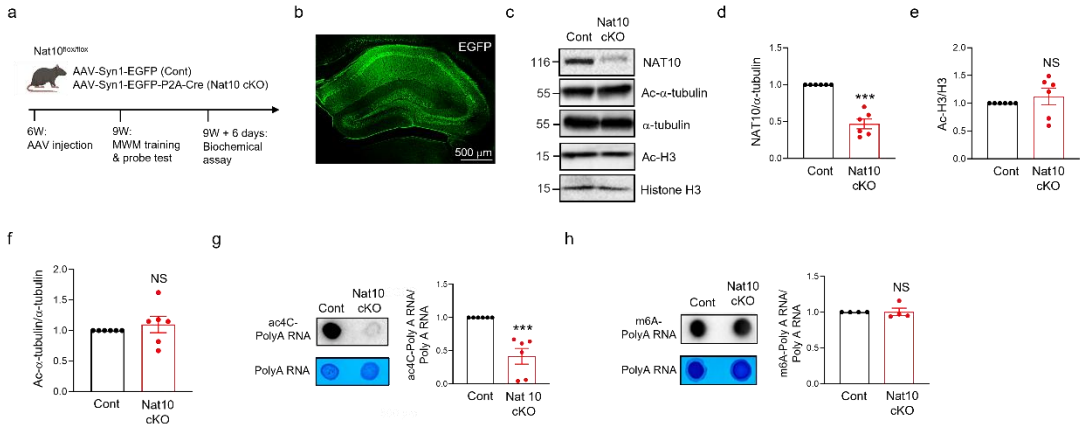

Fig. 5 Regulation of ac4C and protein levels of Arc by NAT10 in SYN after learning and memory. a, Experimental design. Three weeks after AAV injection, the control and Nat10 cKO mice were subjected to MWM training and probe test, and then the

hippocampal tissues were collected for biochemical assays. **b**, Infection of AAV in the dorsal hippocampus. Shown are the fluorescent images of mouse hippocampus expressing EGFP. Scale bar, 500 μm. **c**, Representative images of western blots. The protein samples from control and Nat10 cKO mouse hippocampus were subjected to western blots with the indicated antibodies. **d**, Reduction of NAT10 proteins in Nat10 cKO mice, compared with controls. Shown are quantification data for panel a. n = 6 biological replicates at each condition, *** $P < 0.0001$, two-tailed t-test. Data were normalized by controls. **e**, Similar ac-H3 levels between control and Nat10 cKO mice. Shown are quantification data for panel a. n = 6 biological replicates at each condition, NS, not significant, two-tailed t-test. Data were normalized by controls. **f**, Similar ac-β-tubulin levels in control and Nat10 cKO mice. Shown are quantification data for panel a. n = 6 biological replicates at each condition, NS, not significant, two-tailed t-test. Data were normalized by controls. **g**, Reduction of ac4C in the dorsal hippocampus of Nat10 cKO mice. The mRNA samples were subjected to ac4C dot-blots and methylene blue staining that reveals the total levels of mRNA. Left panel, representative images of ac4C dot-blots and methylene blue staining; right panel, quantification data. n = 6 biological replicates at each condition, *** $P = 0.0006$, two-tailed t-test. Data were normalized by controls. **h**, Similar m6A levels between control and Nat10 cKO mice. The mRNA samples purified from mouse hippocampus were subjected to m6A dot-blots and methylene blue staining. Left, representative images of m6A dot-blots and methylene blue staining; right, quantification data. n = 4 biological replicates at each condition, NS, not significant, two-tailed t-test. Data were normalized by controls.

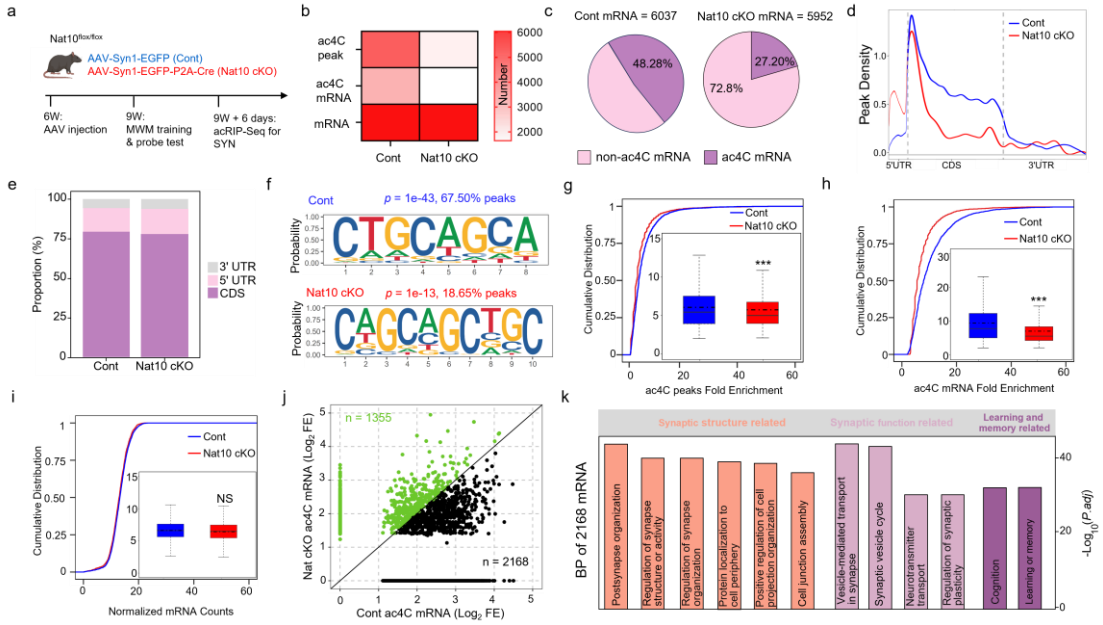

Fig. 6 ac4C sites in the hippocampus of adult mice, and Nat10-mediated effects of ac4C on hippocampal transcriptome. a, Experimental design. Three weeks after AAV injection, the Cont and Nat10 cKO mice were subjected to MWM training and probe test, and then the hippocampal tissues were collected for assays. **b**, The number of ac4C peaks, ac4C mRNA and mRNA between the two groups of Cont and Nat10 cKO mice. **c**, Percentage of ac4C mRNA versus non-ac4C mRNA in both groups. **d-e**, Distribution of ac4C peaks along the different regions of transcripts (d) and genome (e). **f**, De novo motif discovery identified ac4C motif in both Cont and Nat10 cKO peaks, with variation in adjacent nucleotides (99% confidence intervals: Cont target 67.5%; Nat10 cKO target: 18.65%). **g**, Cumulative distribution function (CDF) plot depicting differential fold enrichment of ac4C peaks in Cont vs Nat10 cKO groups. *** P < 2.2e-16, Kolmogorov-Smirnov test. **h**, The fold enrichment of ac4C mRNA between two groups was quantified in the quartile boxplots, where the solid line in the box is the median and the dashed line is the mean, where the maximum and minimum values are identified. *** P < 4.99e-13, Kolmogorov-Smirnov test. **i**, The normalized mRNA counts between two groups was quantified in the quartile boxplots, where the solid line in the box is the median and the dashed line is the mean, where the maximum and minimum values are identified. P = 0.05241, NS, not significant, Kolmogorov-Smirnov test. **j**, Scatter plot of ac4C FE in mRNAs between Cont (x-axis) and Nat10 cKO mice

(y-axis) delineates hyperacetylated (black) and hypoacetylated (green) mRNAs affected by Nat10. **k**, Top 12 biological processes (BP) in which hyperacetylated mRNAs were classified into three major categories (Synaptic structure related, Synaptic function related, Learning and memory related).

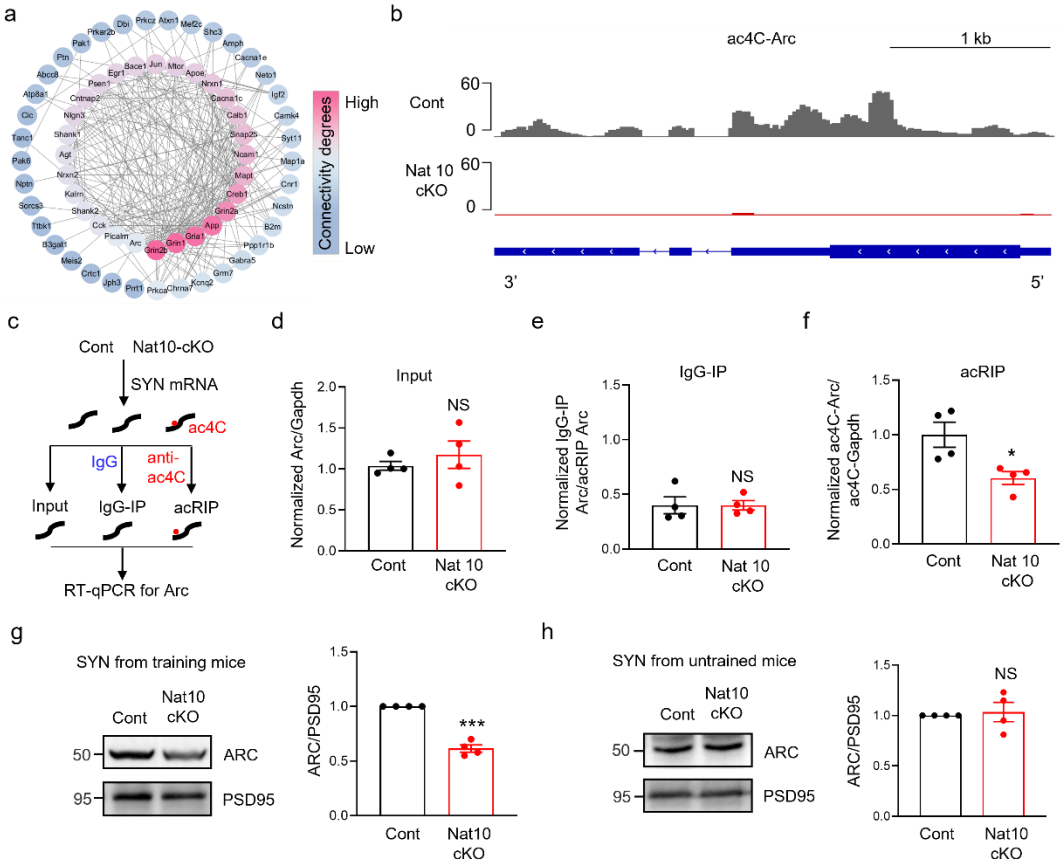

Fig. 7 Regulation of ac4C and protein levels of Arc by NAT10 in SYN after learning and memory. a, The interaction network of genes implicated in learning or memory was constructed using STRING analysis. Nodes in the network are color-coded from pink to purple, indicating genes with low to high connectivity degrees. PPI enrichment, *** $P < 0.0001$. **b**, IGV view of ac4C-Arc in representative NAT10-mediated ac4C mRNA. **c**, Experimental procedure. The SYN mRNA samples of input, IgG-IP, and acRIP from control and Nat10 cKO hippocampus were subjected to RT-qPCR for analyzing Arc mRNA levels. **d**, Arc mRNA levels were not significantly altered in SYN of Nat10 cKO mice, compared to controls. n = 4 biological replicates at each condition, NS, not significant, two-tailed t-test. Data were normalized by controls. **e**, Arc mRNA was detected in the IgG-IP samples. n = 4 biological replicates at each condition, NS,

not significant, two-tailed t-test. **f**, Acetylation of Arc mRNA was significantly reduced in SYN of Nat10 cKO mice after MWM training and probe test, compared with controls. n = 4 biological replicates at each condition, * P = 0.0215, two-tailed t-test. Data were normalized by controls. **g**, Reduction of Arc proteins in SYN of Nat10 cKO mice after MWM training and probe test, compared with controls. The protein samples from SYN of control and Nat10 cKO mouse hippocampus after MWM training and probe tests were subjected to western blots with the indicated antibodies. Left, representative western blot images; right, quantification data. n = 4 biological replicates at each condition, *** P < 0.0001, two-tailed t-test. Data were normalized by controls. **h**, Similar Arc protein levels in SYN of control and Nat10 cKO mice that were not trained in the MWM. The protein samples from hippocampal SYN of control and Nat10 cKO mice without MWM training were subjected to western blots with the indicated antibodies. Left, representative western blot images; right, quantification data. n = 4 biological replicates at each condition, NS, not significant, two-tailed t-test. Data were normalized by controls.

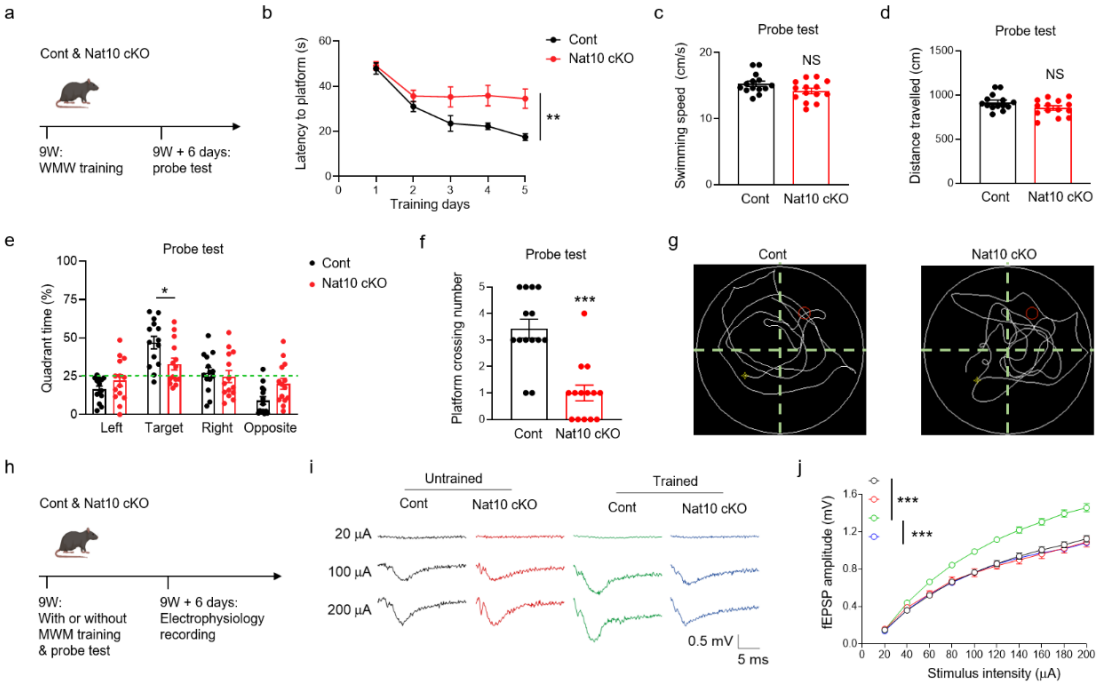

Fig. 8 Regulation of learning and memory by NAT10 in mouse hippocampus. a, Experimental design. The control and Nat10 cKO mice were subjected to MWM training for 5 days, and the probe tests were performed on the 6th day. **b**, Impaired

learning process in Nat10 cKO mice, compared with controls. Shown are learning curves in control and Nat10 cKO mice during training. n = 14 mice per group, *** Genotype $F_{(1, 130)} = 24.08$, $P < 0.0001$, two-way ANOVA followed by Sidak's multiple comparison test. **c-d**, Similar swimming speed (**c**) and distance travelled (**d**) during probe tests between control and Nat10 cKO mice. n = 14 mice per group, NS, not significant, two-tailed t-test. **e**, Time spent in the target quadrant was significant reduced in Nat10 cKO mice during probe tests, compared with controls. n = 14 mice per group, * P = 0.0198, two-way ANOVA followed by Sidak's multiple comparison with post hoc t-test. **f**, Number of platform crossing was significantly reduced in Nat10 cKO mice during probe tests, compared with controls. n = 14 mice per group, *** $P < 0.0001$, two-tailed t-test. **g**, Swimming traces of control and Nat10 cKO mice during probe tests. **h**, Experimental design. The control and Nat10 cKO mice with or without MWM training and probe tests were subjected to electrophysiological recording for assessment of glutamatergic transmission at SC-CA1 synapses. **i-j**, After learning and memory, the glutamatergic transmission at SC-CA1 synapses was significantly reduced in Nat10 cKO mice compared to controls. **i**, Representative fEPSP traces. **j**, Quantification data for panel i. n = 18 slices from 5 mice per group, *** Genotype $F_{(3, 680)} = 128.2$, $P < 0.0001$, two-way ANOVA followed by Sidak's multiple comparison test.

Extended Data Figures and Legends

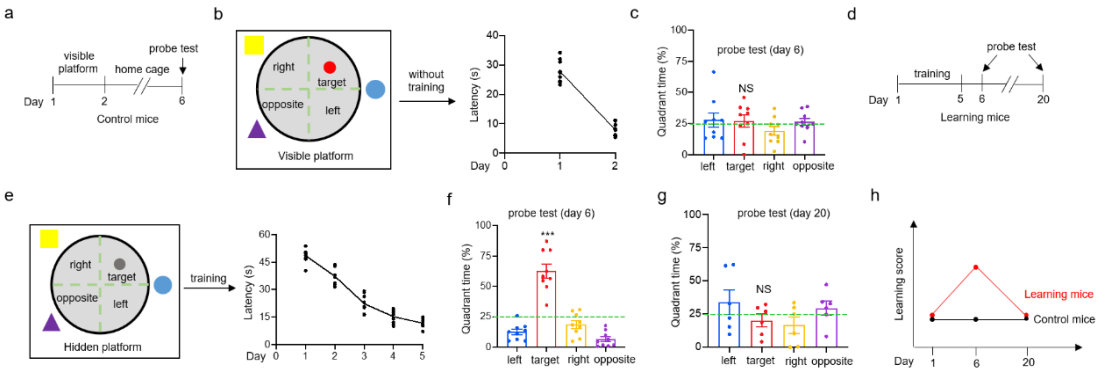

Extended Data Fig. S1 Protocols of Morris water maze (MWM) for control and learning mice. a, MWM protocol for control mice. The control mice were placed in MWM with a visible platform on day 1 and 2, after which they returned to home cage

and were subjected to probe tests on day 6. **b**, Control mice were able to discern the visible platform above the water surface and consequently locate it rapidly. Shown are the latency to find the visible platform on day 1 and 2. **c**, Control mice were not able to remember the target quadrant during probe tests on day 6. Shown are the percentage of time staying in each quadrant during probe tests. n = 9 mice, NS, not significant, one-way ANOVA. **d**, MWM protocol for learning mice. The learning mice were trained in MWM with a hidden platform from day 1 to 5, and then were subjected to probe tests on day 6 and 20. **e**, Learning mice showed improvement in their ability to find the hidden platform during the training process. Shown are the learning curves. **f**, Learning mice could remember the target quadrant during probe tests on day 6. Shown are the percentage of time staying in each quadrant during probe tests. n = 9 mice, *** P < 0.001, one-way ANOVA. **g**, Learning mice could not remember the target quadrant during probe tests on day 20. Shown are the percentage of time staying in each quadrant during probe tests. n = 6 mice, NS, not significant, one-way ANOVA. **h**, Summary of learning scores of control and learning mice on day 1, 6, and 20 after MWM training. Memories were formed on day 6 but were forgotten on day 20 in learning mice.

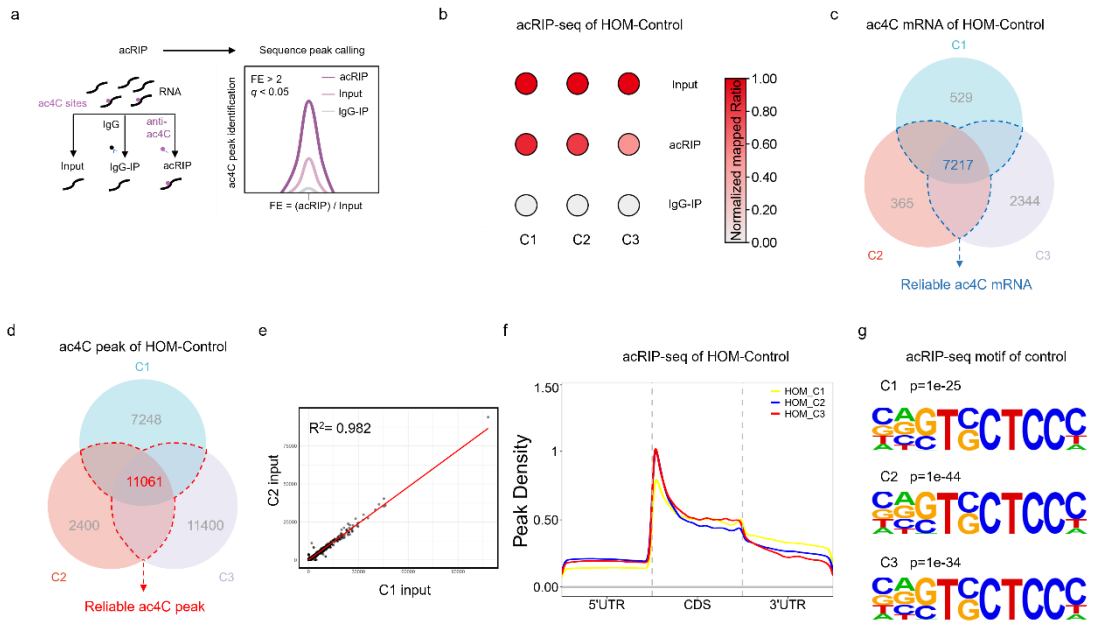

Extended Data Fig. S2 Validation of acRIP-seq and characterization of HOM peaks in the hippocampus of adult mice. a, Workflow of the acRIP-seq protocol. **b**, The dotplot of normalized mapped ratio of IP, Input and IgG among three HOM controls

of acRIP-seq. **c**, The reliable ac4C mRNA identified in at least two biological replicates of HOM. **d**, Peak among reliable ac4C mRNA in three HOM controls of acRIP-seq. **e**, Representative images of pairwise comparison of biological replicate sequencing libraries demonstrates strong, linear correlation between replicates. **f**, Distribution of acRIP peaks along the different regions of transcripts. **g**, Consensus motif and its P value generated by HOMER of the three sets of hippocampal ac4C sites from biological replicates of acRIP-seq.

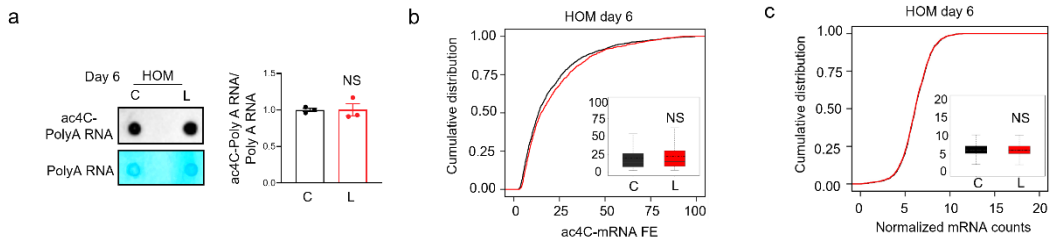

Extended Data Fig. S3 No significant changes in mRNA acetylation in HOM of mouse hippocampus after learning and memory in MWM. a, Acetylation of mRNA was not altered in HOM of mouse hippocampus after memory formation. The mRNA samples used for each ac4C dot-blot were 0.5 μg that falls into the linear range. The HOM mRNA samples of control and learning mice on day 6 were subjected to ac4C dot-blots and methylene blue staining. Left, representative images of ac4C dot-blots and methylene blue staining; right, quantification data. n = 3 biological replicates at each condition, NS, not significant, two-tailed t-test. Data were normalized by controls. **b**, Acetylation levels of SYN ac4C-mRNA were not significantly changed after memory formation in HOM of mouse hippocampus. Shown are cumulative distribution curves of ac4C for HOM LISA in C and L mice on day 6 after MWM training. The ac4C FE of each group was quantified in the quartile boxplots. NS, not significant, Kolmogorov-Smirnov test. **c**, The mRNA levels of SYN ac4C mRNA were not significantly changed in the HOM of the mouse hippocampus after memory formation. Shown are cumulative distribution curves of mRNA levels for SYN ac4C mRNA in HOM of control (C) and learning (L) mice on day 6 after MWM training. The mRNA counts of each group were quantified in the quartile boxplots. NS, not significant, Kolmogorov-Smirnov test.

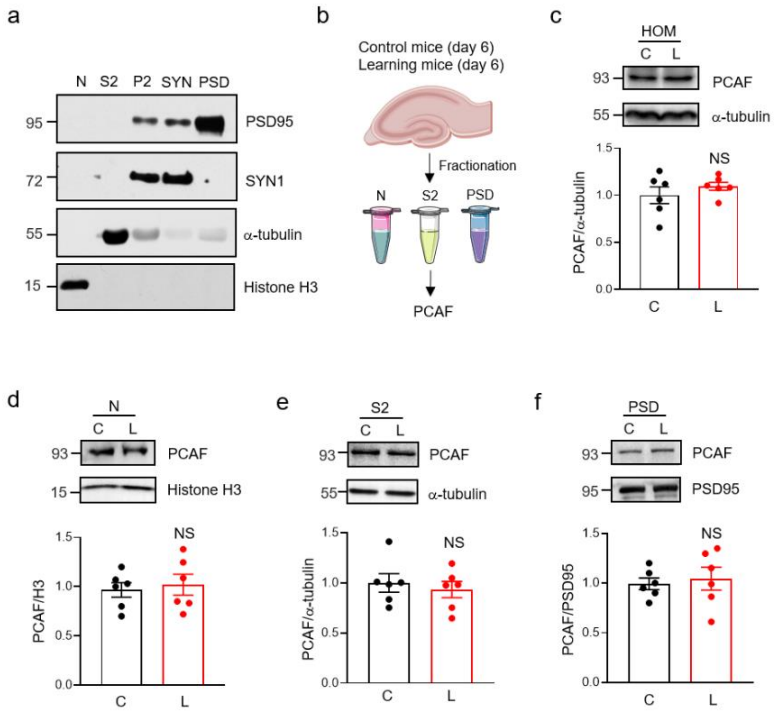

Extended Data Fig. S4 Protein levels of PCAF were not increased in SYN of mouse hippocampus after learning and memory. a, Expression of different protein markers in the N, S2, P2, SYN, and PSD fractions of mouse hippocampus. Shown are representative images of western blots. Protein samples purified from different subcellular fractions of mouse hippocampus were subjected to western blots with the indicated antibodies. **b**, Experimental design. Protein samples were purified from N, S2, and PSD of control and learning mouse hippocampus on day 6 after MWM training, and then protein levels of PCAF were assessed by western blots. **c**, Protein levels of PCAF were not altered in HOM of mouse hippocampus after memory formation. The HOM proteins from control and learning mouse hippocampus on day 6 after MWM training were subjected to western blots with the indicated antibodies. Top, representative western blot images; bottom, quantification data. n = 6 biological replicates at each condition, NS, not significant, two-tailed t-test. Data were normalized by controls. **d-f**, Protein levels of PCAF were not altered in the N (**d**), S2 (**e**), or PSD fraction (**f**) of mouse hippocampus after memory formation. The proteins from different subcellular fractions of control and learning mouse hippocampus on day 6 after MWM training were subjected to western blots with the indicated antibodies. Top, representative western blot images; bottom, quantification data. n = 6 biological

replicates at each condition, NS, not significant, two-tailed t-test. Data were normalized by controls. C, control; L, learning.

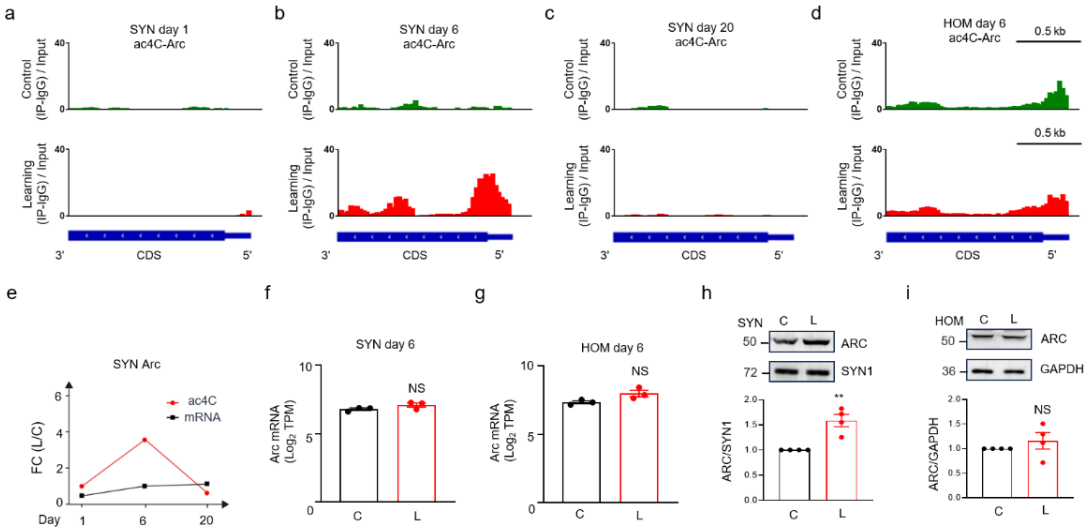

Fig. S5 A representative NAT10-mediated ac4C mRNA for Arc. a-c, Acetylation levels of Arc mRNA were increased after memory formation but returned to normal levels after forgetting in SYN of mouse hippocampus. Shown are IGV diagrams of ac4C peaks in CDS of SYN Arc on day 1 (**a**), 6 (**b**), and 20 (**c**) after MWM training. **d**, Acetylation levels of Arc mRNA were not significantly changed after memory formation in HOM of mouse hippocampus. Shown are IGV diagrams of ac4C peaks in CDS of HOM Arc on day 6 after MWM training. **e**, Quantification data for panel a-c. Shown are FC of ac4C and mRNA levels of Arc in SYN on day 1, 6, and 20 after MWM training. **f-g**, Similar Arc mRNA levels in SYN (**f**) and HOM (**g**) of control and learning mouse hippocampus after memory formation. Shown are logged TPM values of SYN (**f**) and HOM (**g**) Arc mRNA on day 6 after MWM training. n = 3 biological replicates at each condition, NS, not significant, two-tailed t-test. **h-i**, Protein levels of Arc were significantly increased in SYN (**h**) rather than HOM (**i**) of mouse hippocampus after memory formation. The SYN and HOM proteins were extracted from control and learning mouse hippocampus on day 6 after MWM training, and then were subjected to western blots with the indicated antibodies. Top, representative western blot images; bottom, quantification data. n = 4 biological replicates at each condition, ** P = 0.0032 (h), NS, not significant (i), two-tailed t-test. Data were normalized by controls. C,

control; L, learning.

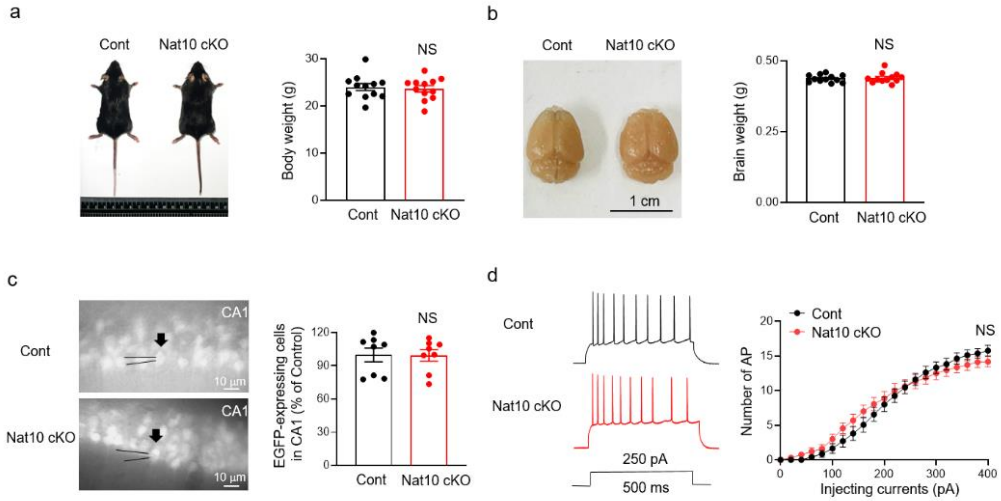

Extended Data Fig. S6 Downregulation of NAT10 in mouse hippocampus does not affect body or brain weight, neuronal number or intrinsic excitability. a, Similar body weight between 10-week-old control and Nat10 cKO mice. Left, representative images of the mice, right, quantification of body weight. n = 12 mice for each group, NS, not significant, two-tailed t-test. **b**, Similar brain weight between 10-week-old control and Nat10 cKO mice. Left, representative images of mouse brain, right, quantification of brain weight. n = 12 mice for each group, NS, not significant, two-tailed t-test. **c**, Similar number of neurons expressing EGFP in the CA1 region of 10-week-old control and Nat10 cKO mice. Left, representative images of CA1 neurons expressing EGFP, right, quantification of EGFP-expressing cells in CA1 region. n = 8 slices from 4 mice, NS, not significant, two-tailed t-test. Data were normalized by controls. **d**, Similar intrinsic excitability of CA1 pyramidal neurons between 10-week-old control and Nat10 cKO mice. Left, representative traces of action potentials (AP) of CA1 pyramidal neurons; right, quantification of AP number after injection of different currents into CA1 pyramidal neurons. n = 20 cells from 4 mice per group, NS, not significant, two-way ANOVA followed by Sidak's multiple comparison test.

a

N=10 mice per seq

Sample	Raw Reads	Clean Reads	Clean Ratio	Q30
SYN-C day 1 Input	45690962	45690826	99.99%	95.99%
SYN-C day 1 ac-IP	34615480	34571324	99.87%	94.83%
SYN-L day 1 Input	40986700	40986580	99.99%	95.93%
SYN-L day 1 ac-IP	35261962	35224988	99.90%	95.47%
SYN-C+L day 1 IgG-IP	28771894	28740616	99.89%	95.61%
SYN-C day 6 Input	50883680	50881302	99.99%	91.41%
SYN-C day 6 ac-IP	42875438	42849170	99.94%	88.50%
SYN-L day 6 Input	44352804	44352528	99.99%	91.43%
SYN-L day 6 ac-IP	42896374	42844138	99.88%	89.85%
SYN-C+L day 6 IgG-IP	42917304	42864638	99.88%	90.81%
SYN-C day 20 Input	39245704	39245602	99.99%	95.67%
SYN-C day 20 ac-IP	33114714	33074726	99.88%	95.10%
SYN-L day 20 Input	37775538	37775450	99.99%	96.08%
SYN-L day 20 ac-IP	31993250	31956866	99.89%	95.19%
SYN-C+L day 20 IgG-IP	34450552	34409158	99.88%	95.25%
SYN-Cont Input	47494076	47485678	99.98%	90.44%
SYN-Cont ac-IP	36251162	34147224	94.20%	91.60%
SYN-Nat10 cKO Input	46660788	46652010	99.98%	90.42%
SYN-Nat10 cKO ac-IP	60886340	40185916	66.00%	86.65%
SYN-Cont+cKO IgG-IP	59704516	41573652	69.63%	90.73%

b

N=3 mice per seq

HOM-C1 day 6 Input	57375292	57372228	99.99%	90.30%
HOM-C1 day 6 acRIP	49838558	49825568	99.97%	90.62%
HOM-L1 day 6 Input	35703564	35702984	99.99%	90.98%
HOM-L1 day 6 acRIP	45501964	45493556	99.98%	90.58%
HOM-C1+L1 day 6 IgG-IP	48075088	48045926	99.94%	92.57%
HOM-C2 day 6 Input	46847176	46846652	99.99%	93.05%
HOM-C2 day 6 acRIP	38929266	38542586	99.01%	90.87%
HOM-L2 day 6 Input	48653096	48652438	99.99%	92.47%
HOM-L2 day 6 acRIP	42074246	41950824	99.71%	88.16%
HOM-C2+L2 day 6 IgG-IP	57469210	42281364	73.57%	87.81%
HOM-C3 day 6 Input	56203128	56200176	99.99%	91.44%
HOM-C3 day 6 acRIP	36085478	36082128	99.99%	90.63%
HOM-L3 day 6 Input	55139518	55138732	99.99%	91.53%
HOM-L3 day 6 acRIP	35343596	35329016	99.96%	89.95%
HOM-C3+L3 day 6 IgG-IP	36754212	36735098	99.95%	90.22%

Extended Data Fig. S7 Library information of acRIP-seq. Samples and quality control information in this study are listed. a-b, The original reads obtained from the sequencing results of SYN samples (a) and HOM samples (b) are raw reads. Clean reads were obtained by removing adapters and low-quality reads from the raw reads. The clean ratio represents the proportion of clean reads to raw reads. The quality of the sequencing data was evaluated using the Q30 metric.